5-1-2009

Mechanical Optimization of Vertical Axis Wind Turbine Blades

Alexander Laurence Combe

LOUISIANA STATE UNIVERSITY

Mechanical Optimization of Vertical Axis Wind Turbine Blades

LSU Honors Thesis

Alexander Combe

5/1/2009

The primary objective of the 2008-2009 Vertical Axis Wind Turbine design team was to improve the overall efficiency of the Vertical Axis Wind Turbine designed by Dr. James R. Bailey and fabricated by the 2007-2008 design team. The turbine design is drag-based and omnidirectional making it capable of producing electrical power regardless of wind direction. It consists of a series of perpendicularly coupled blades that change angle of attack about horizontal axes as rotation about the vertical axis occurs. These combined rotations effectively maximize drag on one side of the turbine while effectively minimizing drag on the opposing side. The design team aimed to improve the overall efficiency of the Vertical Axis Wind Turbine through the mechanical optimization of critical components. A major mechanical optimization technique utilized was to perform an advanced blade geometry analysis. Mathematical modeling and computational fluid dynamics modeling of an array of blade geometries provided theoretical insight as to which blade profile would perform the most efficiently during operation. The resulting Vertical Axis Wind Turbine design entails a more efficient blade profile with superior lift to drag ratios with mathematically predicted behavior. The mechanical optimization of the blade geometry led to significantly improved, aerodynamic blades that obtain a behavior benefitting the performance of the VAWT. However, other factors appear to be negatively influencing the performance of the VAWT in such a manner that the team has been unable to replicate the results obtained by the 2007-2008 VAWT design team.

Table of Contents

Table of Figures

Table of Tables

Introduction

As a youth, the idea of unconventional energy systems stimulated my imagination. The challenge associated with advancing an indistinct concept from the brainstorming stage to the design and implementation stage was an exciting task, yet the relevance of materializing such concepts never seemed completely necessary. Energy was readily abundant for me and I was satiated with light from light bulbs, cool air from air conditioners, and fresh food held in refrigerators. However, I was soon aware after reading and viewing countless news stories that the availability of energy was limited for numerous people globally. The Earth is sliding into an energy and climate crisis. It is imperative to address these issues with focused passion, which means to research and implement nonconventional energy practices. Critics argue that the methods of nonconventional energy sources cannot compete with those of conventional practices. That is true – now. The global market share of renewable energy in 2007 was a meager 6%. However, with major alternative energies demonstrating annual growth of 20% to 50%, it is clear that the renewable global market share is strengthening.

A turbine is a mechanical system that harnesses a percentage of the available energy in an acting working fluid and converts that energy to mechanical rotational energy. The harnessed energy can also be converted into electrical energy through the incorporation of a generator into the operating system. A wind turbine is a system that utilizes the wind as the working fluid and energy source. Most conventional wind turbines maintained and operated in today's society are Horizontal Axis Wind Turbines (HAWTs) meaning that the blades or vanes rotate about an axis that is horizontally oriented. HAWTs have proven to have a few limiting operating constraints, especially the facts that they are instantaneously unidirectional and require a large open area in which to operate efficiently. A gearbox and control system must be incorporated into a HAWT in order to change the radial direction of the horizontal axis in order to properly absorbed energy from the wind.

Dr. James R. Bailey's proposed design of a new Vertical Axis Wind Turbine (VAWT) has been submitted to the United States Patent and Trademark Office for approval. The VAWT design addresses the inherent problems associated with Horizontal Axis Wind Turbines. One of the positive aspects of this vertical system is that the turbine will properly operate for all possible wind directions (i.e., it is an instantaneously omnidirectional wind turbine), unlike a horizontal axis wind turbine. The underlying theme behind Dr. Bailey's proposed design can be traced back to the most efficient of the conventional vertical axis wind turbines currently utilized in the wind energy arena, the Savonius VAWT. The Savonius VAWT consists of two hollow semi-cylinders demonstrating eccentricity about the rotating vertical axis. One side of the Savonius has an effective high drag, due to the cup geometry, and the other side has an effective low drag side, due to the smooth round surface over which the wind can pass.

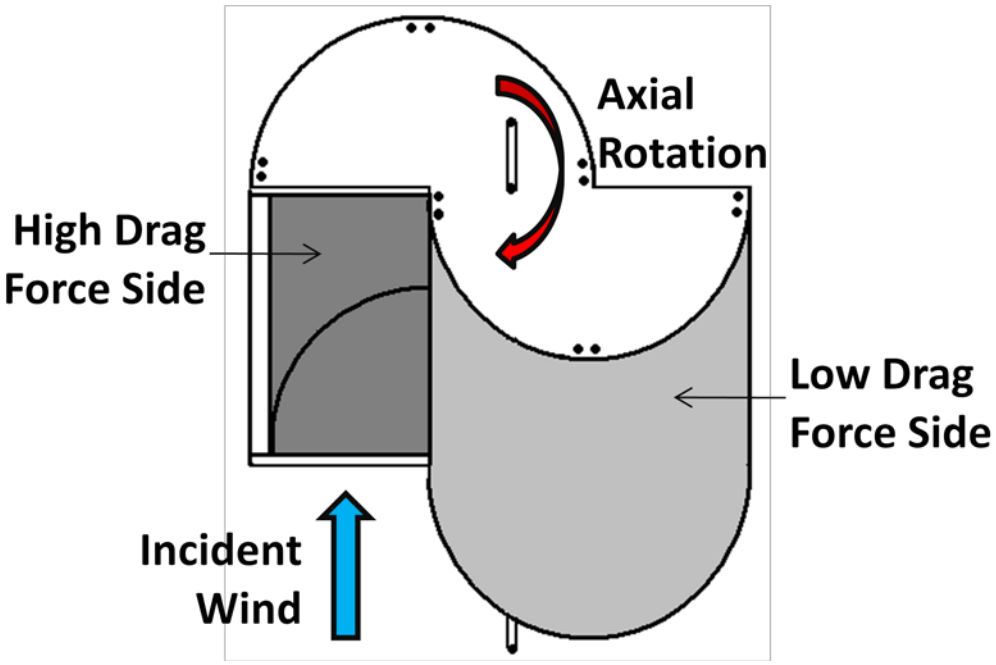

Figure 1: Savonius VAWT Schematic [9]

Dr. Bailey's ideation led him to design a system that also has high and low drag force sides; however, his interpretation essentially utilizes a flat plate perpendicular to the wind, which represents the high drag force side, and a set of flat plates parallel to the wind, which represents the low drag force side (Figure 2).

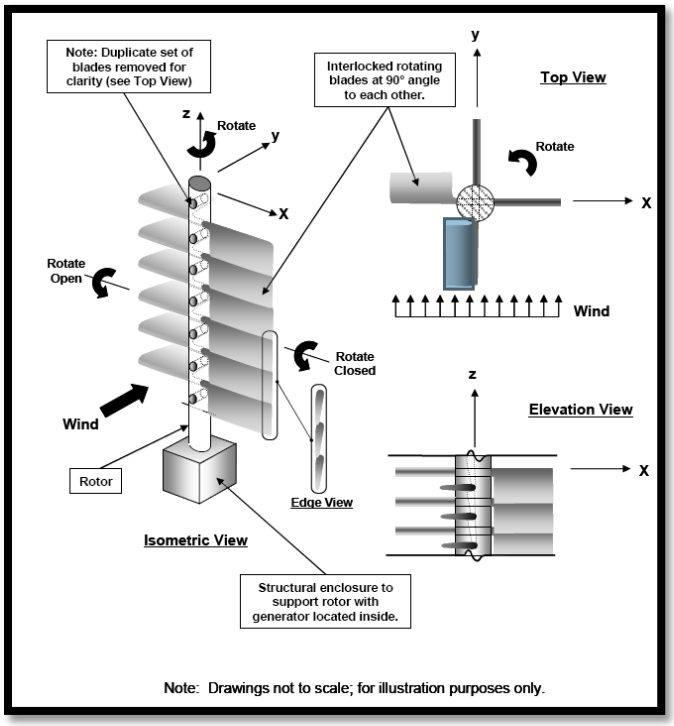

Figure 2: Dr. James R. Bailey's Original Concept (Courtesy of Dr. James R. Bailey)

Last year's team designed and produced a working VAWT based on a conceptual design by Dr. Bailey. Their testing results and data analysis helped the 2009 VAWT team to further advance the VAWT system design in the preliminary design stages. This year the design team aimed to improve the conversion of mechanical to electrical energy of the system through mechanical optimization, thus ultimately improving the overall efficiency of the system. This year's design team benefited by working in several areas, the most important of which being the dynamic characterization and mathematical modeling of a flat plate blade geometry, and computational fluid dynamic modeling and aerodynamic analysis of several blade geometries. Secondary optimization was addressed by the design team through advanced materials selection for blade materials, improved fabrication of turbine blades, and several other techniques.

By increasing the overall turbine efficiency, Dr. Bailey's concept for a new VAWT has the potential to make wind turbines a legitimately viable option as an energy source on the residential scale as well as become more economically feasible. The successful design of the project could lead to more research and possible commercial development aimed at residential use for this type of VAWT. With an increase in the overall efficiency and given the inherent ability to operate within more liberal constraints, the vertical axis wind turbine will better contend with its horizontal axis competitors.

Characterization of 2008 Prototype Behavior

In order to begin improving the efficiency of the vertical axis wind turbine it was critical to understand the dynamic behavior of the current design. Several aspects of the design were important to characterize. These design characteristics included the position, velocity, and acceleration relationships of the blades incorporated into the turbine design. Figure 3 demonstrates the standardization of defining turbine position that the 2009 VAWT design team followed.

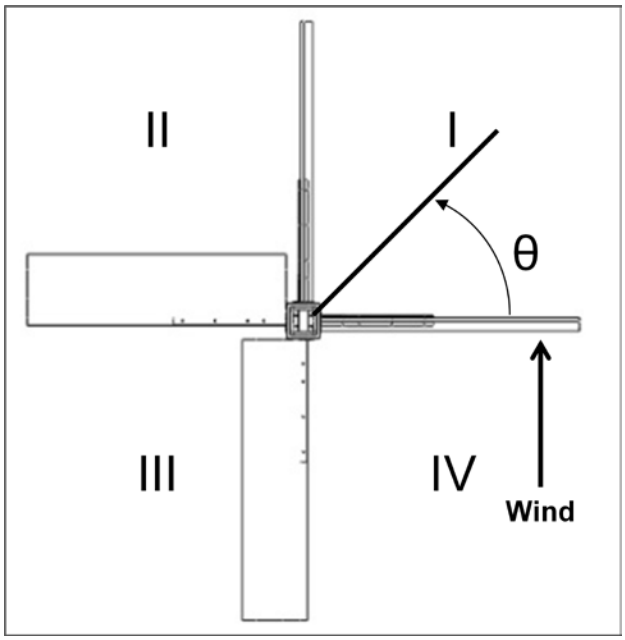

Figure 3: Standardized Orientation about θ Axis

Another important intricacy of the vertical axis wind turbine system that was necessary to characterize involved the forces acting on the blades and rotating shaft during system operation. Data from the 2008 VAWT team as well as the design incorporating the flat plate blade geometry was utilized to characterize the behavior of the existing design. Utilization of this data made it possible to perform a regression analysis that defined the speed of the turbine as a function of wind speed. Linear regressions were used because such regressions were sufficient enough to characterize the relationship between rotor RPM and wind speed. The function is defined in Equation 1.

Equation 1: $$\boldsymbol{RPM = 3.92 * V - .427}$$

where:

V = Wind speed in miles per hour

An average of all the developed linear regressions provided an approximate relationship for the turbine RPM as a function of wind speed in miles per hour (Figure 4).

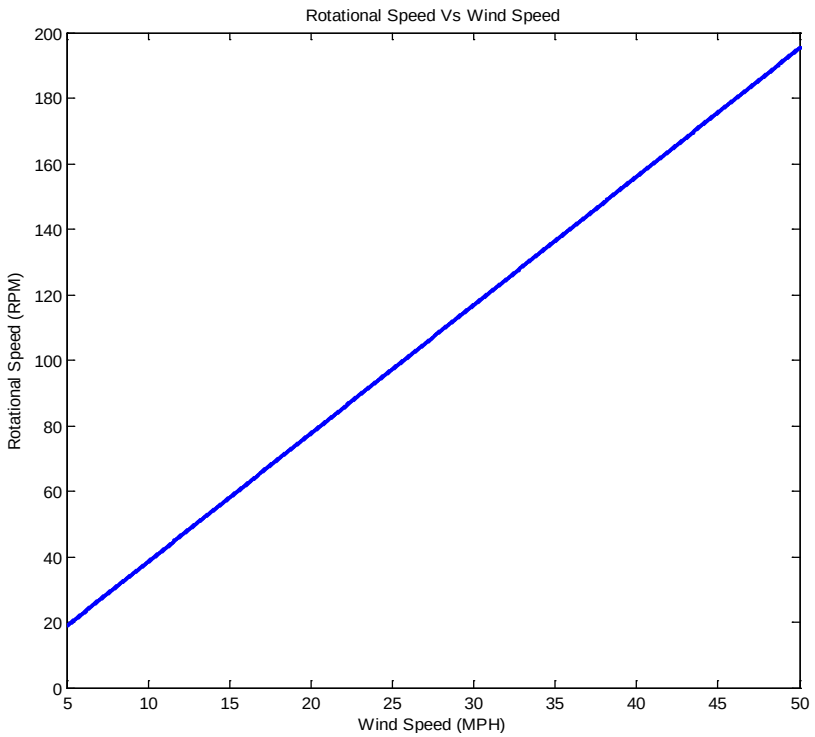

Figure 4: RPM as a Function of Wind Speed

For all calculations and reference purposes it should be noted that θ and $\dot{\theta}$ represent the angular position and velocity about the axis of the main rotor shaft. Similarly, ϕ and $\dot{\phi}$ denote angular positions and velocities, but about the axis of rotation of the connecting rods to which the coupled blade pairs are attached. ϕ is defined to be 0 degrees when the blade is in the closed position and -90 degrees when in the open position ($-90 \leq \phi \leq 0$; i.e., $\phi = 0°$ when the blade represents a flat plate perpendicular to the incident wind field and

$\phi = -90°$ when it represents a flat plate parallel to the incident wind field). The relationship between θ and ϕ has been characterized as a piecewise relationship due to the presence of a stopping mechanism.

In order to mathematically characterize the relationship between ϕ and θ, aerial footage was taken of the 2008 model at various wind speeds. The video was then analyzed frame by frame to obtain a series of data points that related the position of ϕ to the position of θ and also wind speed. Using these data sets, series of regressions were completed to depict the ϕ position as a function of θ. Also, a plot was generated to depict the steady and transient states of ϕ for the flat plate blade geometries at various wind speeds. The plot can be seen below in Figure 5.

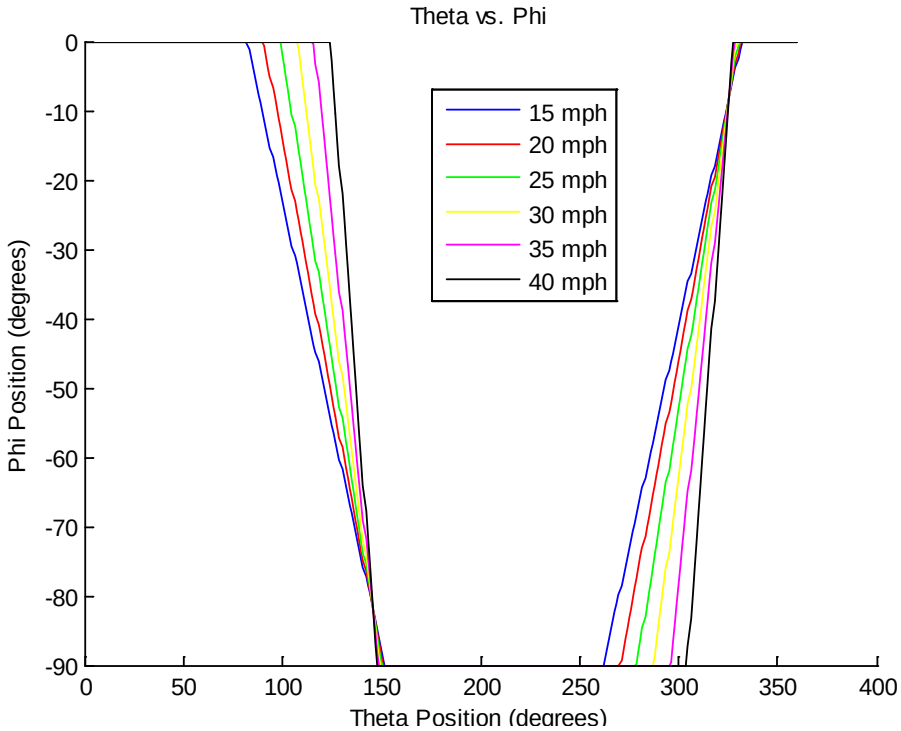

Figure 5: ϕ as a Function of θ

The behavior of the blades shown in Figure 5 is piecewise because of the stops that are designed to constrain the motion in the ϕ direction. From Figure 5 it can be seen that as the wind speed increases the transition period occurs more quickly. This is an expected result because of the greater angular momentum of the turbine rotor due to the greater RPM that the turbine will be experiencing. It is important to note that at low speeds the blades begin to open before $\theta = 90$ degrees, but at increased wind speeds the blades begin to open at angles exceeding $\theta = 90$ degrees, which can also be contributed to the increased angular momentum of the turbine shaft due to increased RPM. At all of these wind speeds, however, it can be seen that the blades reach their steady state open position at an approximate angle of $\theta \approx 150°$.

Another major aspect of the analysis on the 2008 VAWT design was completed by assuming that the transient states of ϕ have a constant angular velocity (i.e., $\phi = Constant$). This made it possible to obtain the angular velocity of the turbine rotor as a function of wind speed (Figure 6).

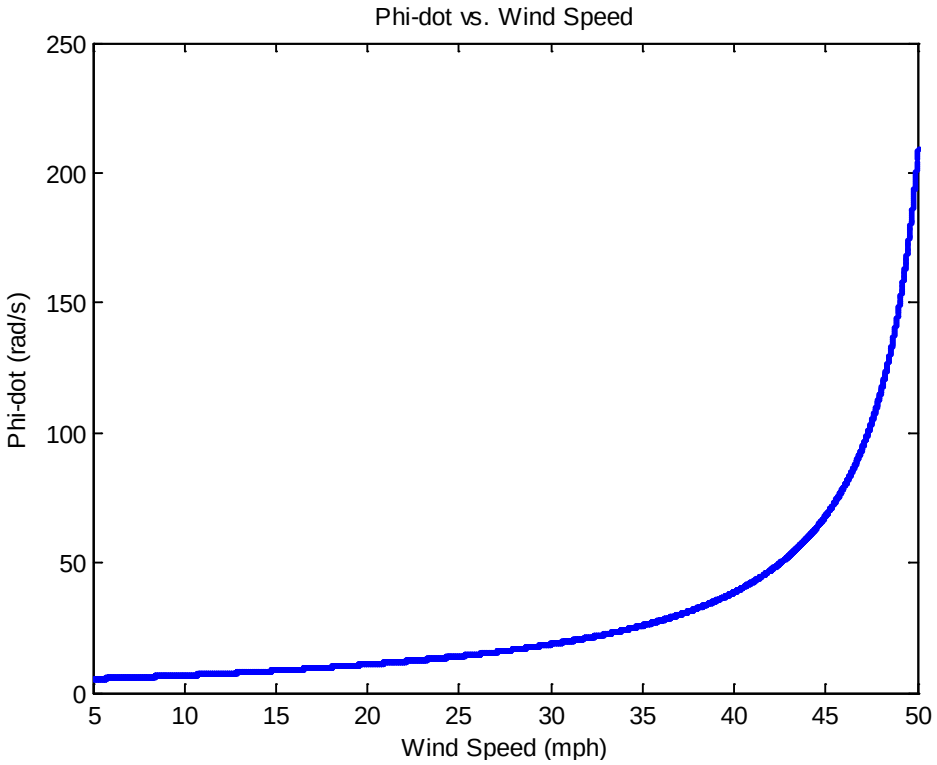

Figure 6: $\dot{\phi}$ vs. Wind Speed

Utilization of this analysis from the methods mentioned above allowed for the approximate characteristic relationship of the motion of the turbine blades and turbine rotor as a set of functions of wind speed to be fully characterized and comprehensible.

Dynamic Analysis

An integral part of the blade geometry analysis and design of the VAWT was to derive the equations of motion that govern the mechanical system. The motion of the VAWT is extremely unique because of the rotation about two axes as opposed to just one and because of the dependence of the two rotations upon one another. Since the angle of rotation of the system about an established origin (i.e., $\theta = 0°$) directly influences the angle of rotation of the blades, it also determines the magnitude of the forces that act on the system. The forces acting on the blades change dynamically as the angle of attack of the blades changes. In addition, the center of pressure, or the point of application that the forces act upon, is also dynamically changing and affecting the system in different ways.

In order to model the motion of any point on the VAWT, Newtonian mechanics were utilized along with generalized position vectors. The position vector is dependent on the angles of rotation θ and ϕ about the θ and ϕ axes, respectively (Figure 7). The position vector ($r_{P/O}$) is defined with respect to a stationary coordinate system at the base of the VAWT and is demonstrated in Equation 2.

Equation 2: $$\boldsymbol{r_{P/O_1} = (x\cos\phi\cos\theta - z\sin\phi\cos\theta - y\sin\theta - R\sin\theta)\hat{\imath} + (x\cos\phi\sin\theta - z\sin\phi\sin\theta + y\cos\theta + R\cos\theta)\hat{\jmath} + (-x\sin\phi - z\cos\phi + L)\hat{k}}$$

where,

$R = Radius\ of\ the\ shaft$

$L = Height\ of\ minor\ axis\ of\ blade\ from\ origin, O_1$

$x, y, z = Coordinates\ on\ blade\ referenced\ from\ blade\ origin, O_3$

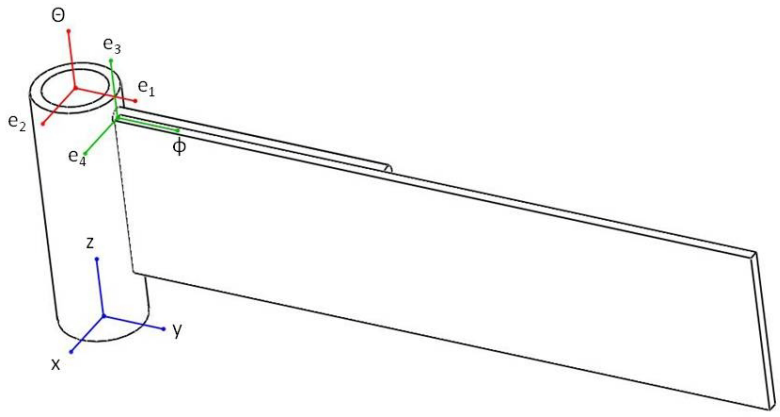

Figure 7: Orientation of Axes Used in Dynamic Analysis [7]

Figure 8 on the following page is a *MATLAB* plot illustrating the four corners of a flat plate blade geometry during one revolution of the turbine shaft about the θ axis. This plot was generated from a code that was written before the code for Figure 5 was generated. An assumption is included in the code in which ϕ changes about the axis of the connecting rods at a directly proportional rate of 1:1 for changes in θ about the vertical axis. Therefore, for every degree of rotation of the shaft about the vertical axis the blades also rotated one degree in the same period of time. It is important to note that that transient states of the blades occurred between quadrants 2 and 4 and steady state position of the blades occurred between quadrants 1 and 3 as defined in Figure 3.

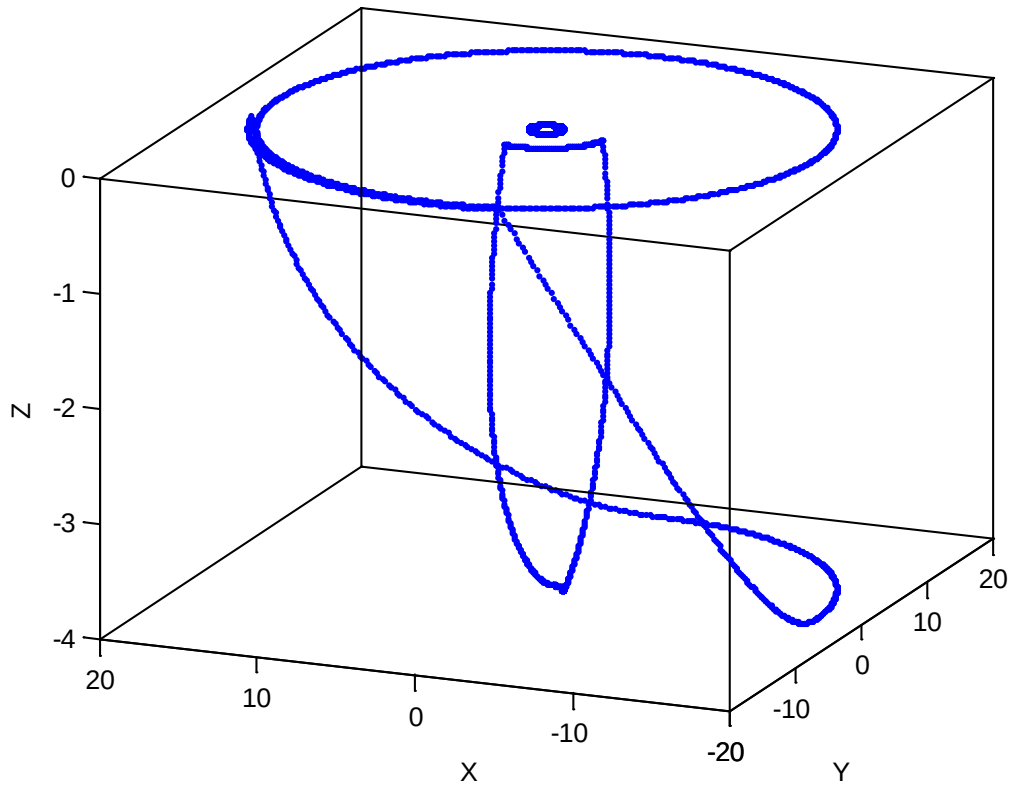

Figure 8: *MATLAB* Plot of Corners of Flat Plate Blade Geometry about θ Axis

Differentiation of Equation 2 with respect to time once and then twice, the velocity and acceleration vectors were obtained, respectively. Of these three derived vectors, the velocity vector was the most critical to the optimization of the VAWT. It was important because it allowed the determination of the absolute velocity of any point on a blade at any given time. The absolute velocity of a point can then be combined with the wind velocity to find the relative velocity of a point with respect to the wind.

Knowledge of the relative velocity of the blade with respect to the wind was crucial in the characterization of the lift and drag forces acting on a blade. As the blades rotate in the same direction as the wind flow the relative velocities will be significantly lower than when the blades rotate against the incident wind flow. Because the lift and drag forces exerted on a blade are a function of the velocity squared, both will theoretically be more greatly influenced on the side of the turbine that is cutting into the wind. Since angular velocity can be converted into translational velocity based on radius, each point on a blade has a different absolute velocity; therefore, every single point on a blade experiences different lift and drag forces at all times. A sensible assumption that the velocity of the center of the blade be used to characterize the lift and drag forces for the entire blade was made for convenience and ease of calculation. Since the velocity would be linearly distributed this assumption is justified by the fact that the center of the blade travels at the average velocity of the entire blade.

In order to calculate the lift and drag forces exerted on a blade at any given position, the coefficients of lift and drag for that position need also be known. Standard lift and drag coefficients for a flat plate blade geometry are well known for angles of attack within the operating range of ϕ. However, very little published

data cites lift and drag coefficients for rotations about the θ axis. Due to this complication an assumption was made that the rotation about the θ axis would not significantly affect the lift and drag coefficients. Obtaining accurate values for various angles about the ϕ axis was achieved by thorough research on flat plate behavior and airfoil behavior at various angles of attack. The National Advisory Committee for Aeronautics (NACA) has immense amounts of published data on airfoil behavior at every angle of attack about the ϕ axis from 0 to 180 degrees [1 & 2]. Also, flat plate aerodynamic data is well published for various aspect ratios, and research proved that airfoils act like flat plates at angles of attack that happen to be greater than the stall angle ($\phi \approx 15°$). A compilation of the vast amount of researched information led to the creation of a spreadsheet that provided polynomial regressions of lift and drag profiles at various aspect ratios.

The regressions from Figure 5, which demonstrates the detailed relationships between the angle of attack of the turbine blades and the turbine angular displacement, were necessary for proper use of the spreadsheets mentioned previously. Iterative processes were utilized in *MATLAB* to constantly call on the regressions and correct the instantaneous lift and drag coefficients for two sets of perpendicularly coupled blade pairs. These iterative processes were necessary because of the dynamic nature of the VAWT and the coupled relationships between ϕ and θ.

To perform a force analysis on the VAWT it was important to note that only three forces act on the system. Two forces previously mentioned that act on the system are the lift and drag forces due to the blades. The third force that acts on the VAWT is the weight of all of the blades and coupling rods. Besides these three forces the only other considerations are the impact forces from the blades closing on each other and the resistance torque present from the generator, which can both be considered internal to the system. These forces govern all of the motion that the VAWT experiences.

Analysis on the effect of different wind speeds on the VAWT meant that the wind must first be converted to forces. As previously stated the only forces that occur from the wind are lift and drag forces on each blade. *MATLAB* was utilized to iteratively apply all of the forces present at any time. Important aspects of the lift and drag forces that were derived from the dynamic analysis of the system include the relative velocity of each blade and the projected area at any given time. Utilizing all of this information a program was written that performs the summation of moments about the θ and ϕ axes and subsequently sets up a governing differential equation of motion for the VAWT. Since there are two axes of rotation for the VAWT there are two coupled, governing, ordinary differential equations. The governing equation for the motion about the ϕ axis is piecewise due to the stopping force that acts on the blades as they close upon one another. The piecewise behavior of the blades greatly increases the difficulty of solving the ordinary differential equations that govern the vertical axis wind turbine motion. A complete solution of the coupled, ordinary differential equations has not been determined, though numerical methods were attempted as an alternative to achieve approximate solutions to the problem. The analysis process was completed by constraining the motion of the VAWT to times when the blade was already stopped. This method of analysis was utilized for an array of aspect ratios as a means to determine the optimum aspect ratio for the optimum blade geometry.

Aspect Ratio

The 2008 design team's turbine blades were simply a flat plate with an aspect of ratio of 4:1, where aspect ratio can be defined as the width of the blade over the height of the blade. Last year's design team

finalized blade dimensions at a width of 16 inches and a height of 4 inches, thus arriving at the aspect ratio mentioned previously [6]. Optimization of the aspect ratio was viewed as a necessity and was one of the earliest objectives of the design process. Simple calculations utilizing force balance equations proved to be ineffective for optimizing the aspect ratio. Each solution simply stated that the optimum aspect ratio was infinity (resulting in a large swept area) or zero (resulting in a nonexistent drag on the open side). These solutions are trivial and proved a simple balance of equations as unacceptable for selecting aspect ratio. After a complex dynamic modeling program code was written in *MATLAB* it was possible to vary the aspect ratio of a theoretical set of coupled blades from 1 to 20 and evaluate the critical wind speed at which the blades achieved the fully closed position ($\phi = 0°$). The results of that simulation are shown on the following page.

	mph
W=16"	Wind Critical=22.1 AR= 1
	Wind Critical=23.1 AR= 2
	Wind Critical=23.0 AR= 3
	Wind Critical=22.9 AR= 4
	Wind Critical=22.9 AR= 5
	Wind Critical=22.8 AR= 6
	Wind Critical=22.8 AR= 7
	Wind Critical=22.8 AR= 8
	Wind Critical=22.8 AR= 9
	Wind Critical=22.8 AR=10
	Wind Critical=22.7 AR=11
	Wind Critical=22.7 AR=12
	Wind Critical=22.7 AR=13
	Wind Critical=22.6 AR=14
	Wind Critical=21.8 AR=15
	Wind Critical=22.6 AR=16
	Wind Critical=22.6 AR=17
	Wind Critical=22.6 AR=18
	Wind Critical=22.6 AR=19
	Wind Critical=22.7 AR=20

Table 1: Critical Wind Speed for Various Aspect Ratios

The data in Table 1 demonstrates that a significant change in the aspect ratio of a theoretical set of coupled blades obtaining flat plate blade geometries results in a minimal change in the critical wind speed, or the wind speed required to achieve the fully closed position of one of the blades in the coupled pair. A change in the aspect ratio of the blades would not have significant implications on the performance of the turbine; however, changing the aspect ratio would cause significant repercussions on overall mass of the turbine as the number of components would be greatly increased to achieve the final assembled design. Also, the increase in components would prove to be a detriment on the ease of fabrication of the turbine were it to become commercially

producible. In light of these unfavorable effects of varying the aspect ratio to the optimum, it was determined that the existing aspect ratio of 4:1 should be kept as a means of easy fabrication, but also in order to perform thorough comparisons between the flat plate blade geometries and the potential substitutes to be mentioned later.

Ultimately, the purpose of the dynamic and force analyses was to optimize the blade dimensions. It was crucial to determine which blade dimensions will produce the greatest combination of lift and drag forces that will in turn result in the greatest net force and net moment values about the main turbine shaft.

Tip Speed Ratio

After analysis of the data provided by the 2008 design team, one major concern existed regarding the goal of improving the overall efficiency of the turbine. Their data from prototype testing demonstrates that the efficiency of their turbine obtained a maximum value at a wind speed of approximately 22 miles per hour. The reason that efficiency began to fall at this point is because the tip speed ratio, which is the ratio of the linear speed at tip of the blade to incident wind speed, ceased to rise and, in fact, began to fall from its peak of approximately 0.37 (Figure 8). In order to achieve the optimum efficiency of drag based vertical axis wind turbines the tip speed ratio should be as close to 1 as possible, if not greater. The fact that the tip speed ratio did not rise above 0.40 and actually falls at increased wind speeds introduces adverse affects upon the efficiency of the VAWT.

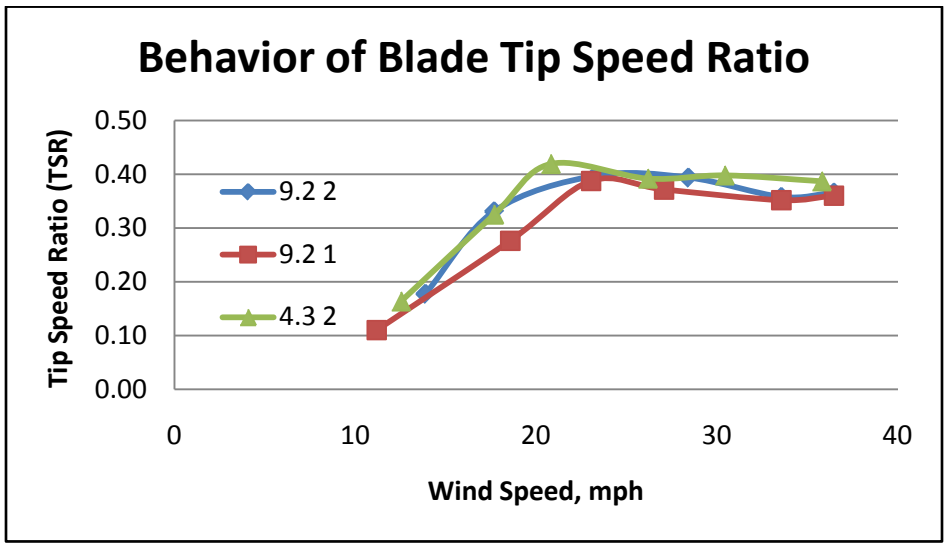

Figure 9: Behavior of Blade Tip Speed Ratio at Various Wind Speeds [6]

It has been generalized that there may exist a wind speed at which the unsteady nature of the wind field in the wake of the turbine will limit the VAWT to have an undesirable maximum tip speed ratio much lower than 1. The unsteady nature of the wind field can be attributed to the trailing vortices from the vertical series of blades and their rather violent and broad change of their angle of attack. The turbine may in effect be causing so much turbulence that it is operating within its own wake, thus potentially contributing to significant losses in the overall efficiency. The wake causes lift and drag data to be inaccurate and, therefore, force data to be inaccurate. If this conjecture is proven accurate, the issue may not be able to be resolved by blade design alone.

However, to address this issue it would be necessary to perform a flow-structure interaction analysis through CFD software. This process requires very powerful computers and unprecedented amounts of research time. Due to these conditions this was not further analyzed.

Blade Design

One area of the turbine design in which the team attempted to significantly increase the efficiency was through effective blade design, despite the potentially limiting turbulence previously mentioned. The blades are the primary components responsible for the extraction and transmission of energy from the wind to the main shaft. In order to significantly increase the efficiency of the turbine the team theorized that the blade geometry needed to be optimized in such a way that the drag force on the open side of the turbine would be decreased while the drag force on the closed side of the turbine would be increased. This optimum blade geometry would primarily be a function of the blade cross section, or the blade profile, and the aspect ratio of the blade though variable cross sections could have been incorporated in order to obtain prominent characteristics of multiple geometries in a single blade. In order to instantaneously maximize and minimize the drag on the closed and open sides of the turbine, respectively, it is desirable to have each coupled blade pair transition rapidly from the closed to open position, and vice versa.

Computational Fluid Dynamics (CFD)

The team decided to incorporate CFD to help determine the optimum blade geometry from an array of preselected geometries as well as test the hypothesis that maintaining the aspect ratio of 4:1 would not significantly hinder the performance of vertical axis wind turbine. The set of blade geometries were chosen because of the foreseen ease of fabrication relative to the allotted time and budget that the design team was presented with. In order to accomplish this complex analysis, CFD software had to be selected. The two programs at the disposal of the design team were *FLUENT* and *ANSYS* and both software packages demonstrate extreme levels of functionality regarding solving problems of complex nature. One advantage of utilizing *ANSYS* would have been the design team's ability to run flow-structure interaction (FSI). This feature of *ANSYS* allows for the user to view simulated real time motions due to theoretical external fluid interactions. FSI would have allowed the design team to perform simulations where observations of the deformations of the blades as well as the rotational motion about both axes caused by specific wind loads on the VAWT could be made. The design team could have also potentially studied the possible presence of severe turbulence near the rear of the turbine ($70° \leq \theta \leq 110°$) and the effect on subsequent blade couples that would be entering the unsteady field. The main disadvantage of *ANSYS* was the fact that the LSU Student License did not allow for the program to be run on parallel processors. The Student License of *FLUENT* did however allow the use of parallel processors; therefore the team decided to utilize *FLUENT* as the CFD software. The team also decided to use *GAMBIT*, a program used to build and mesh geometries that are to be imported into *FLUENT* for complete analysis.

Two dimensional *NACA 0015* and flat plate blade geometries were built and analysis was run on them as a means of verifying *FLUENT* was returning appropriate coefficients of lift and drag at specific angles of attack. This would allow the team to gain an understanding of *GAMBIT* and *FLUENT* and select a proper turbulence model for the blade CFD. While running 2-D cases, the team learned that it was necessary to run a steady case, followed by an unsteady case for blades at high angles of attack. The unsteady model would account for

shedding vortices behind the blade, a phenomenon that greatly affects the coefficients of lift and drag. Shedding vortices can be seen in the following picture of velocity contours of a *NACA 0015* at an angle of attack above the stall angle.

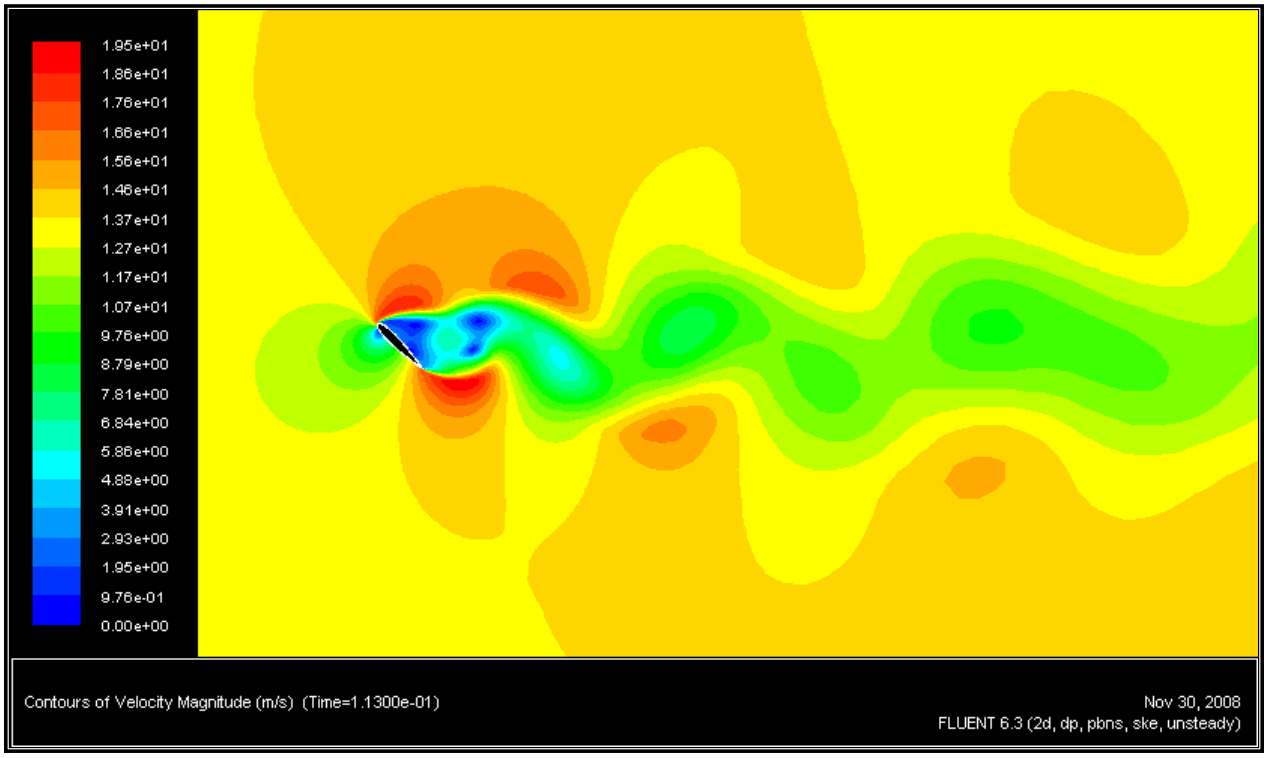

Figure 10: *NACA 0015* Velocity Contours (α=65°) [7]

Several turbulence models were tested when modeling the VAWT blades. The first model used was the standard k-ε turbulence model. This is one of the most commonly used turbulence models, and the team felt that it would produce accurate results. While the k- ε model proved to be accurate, after researching other models, the team decided to use the SST k-ω turbulence model. This model was known to produce accurate results for low Reynolds number flow and large separation, two qualities of the flow over VAWT blades.

After an appropriate turbulence model was selected, the team began three dimensional modeling of the VAWT blades. The purpose of the 3-D model was to allow the team to change both the angle of attack and the angle of rotation about the vertical shaft. This would more accurately represent the VAWT blades when solving for the coefficients of lift and drag. From Equations 1 & 2 derived earlier, a complex *MATLAB* code was written from the equations of motion for the flat plate coupled blade pairs that solved for the angular position, angular velocity, projected area, and relative velocity of the center of mass of a blade (The four values solved for were θ, ϕ, A_{proj},and V_{rel}). This code provided the team with the necessary information *FLUENT* required in order to complete a CFD analysis for each blade position. The accuracy of the values of lift and drag coefficients for each blade was expected to demonstrate some error as the equations for the transient motion of the blades about the ϕ axis were approximated linear regressions. However, as mentioned earlier, these regressions provided sufficiently accurate approximations of the values of ϕ as a function of wind speed and angular position of the shaft, θ. Also, because the team was utilizing *FLUENT* in order to determine the lift and drag coefficients of

several different blade profiles and not only the flat plate design, some error was expected for the coefficients of alternative blade geometries. Alternative blade geometries would not follow exactly the dynamic motion of a flat plate blade geometry; however, since airfoils behave as flat plates at angles of attack beyond their stall angle that the *MATLAB* code solutions could also be utilized for the various other blade geometries entered into *FLUENT* for analysis.

The objective of blade optimization was to create a blade geometry that maximized drag on the closed side and maximized lift while minimizing drag on the open side. Introducing lift to the open side of the turbine will aid the blades in staying closed longer on the high drag side of the turbine. The relative velocities of the center of mass of the blades were used as velocity inlet boundary conditions in *FLUENT*. A complex velocity profile is extremely difficult to model in *FLUENT* and therefore bolstered the team's decision to utilize the relative velocity of the center of mass as a constant velocity inlet. Also, the team considered modeling the unsteady flow that the blades actually encounter but decided that for comparison purposes laminar flow inlets were sufficient.

Several blade geometries were created in *GAMBIT* to compare to last year's flat plate design. A 3-D model was created and meshed for each blade profile at every 20 degrees of rotation about the θ axis with the appropriate rotation about the ϕ axis incorporated as well. The first 3-D model to compare to the flat plate was a *NACA 0015* profile. It was anticipated that this symmetrical airfoil design would significantly reduce the drag on the open side of the turbine while minimally affecting the drag on the closed side. The team also created a flat plate with a scooped end to test in *FLUENT*. It was anticipated that while in the closed position, a blade with a scooped end would have an increased drag as the turbine rotated (i.e., as $\theta \rightarrow 90°$). The team also noted that the scooped end would not have a significant impact on the open side drag of the turbine. Two scooped ends were tested in *FLUENT*. The first profile consisted of a flat plate with a minor scoop at the end (a height of 1 inch), while the second was created with an exaggerated scoop (a height of 2 inches). Two scooped profiles were tested in *FLUENT* to find what role scoop size had in affecting the lift and drag coefficients of the blade. The final geometry tested in *FLUENT* was a cambered flat plate. A consensus was reached among team members that a cambered plate would significantly increase the lift on the open side of the turbine. A cambered plate is also easier to manufacture than an airfoil as the thickness of the plate is constant and that of an airfoil is not. The cambered plate was modeled after the camber line of the *NACA 4415* profile. The *NACA 4415* profile demonstrates minimal drag at 0 degrees angle of attack while maintaining a significant lift. It was anticipated that this profile would benefit the closed side of the VAWT by providing a lift force on the open side to keep the blades shut longer.

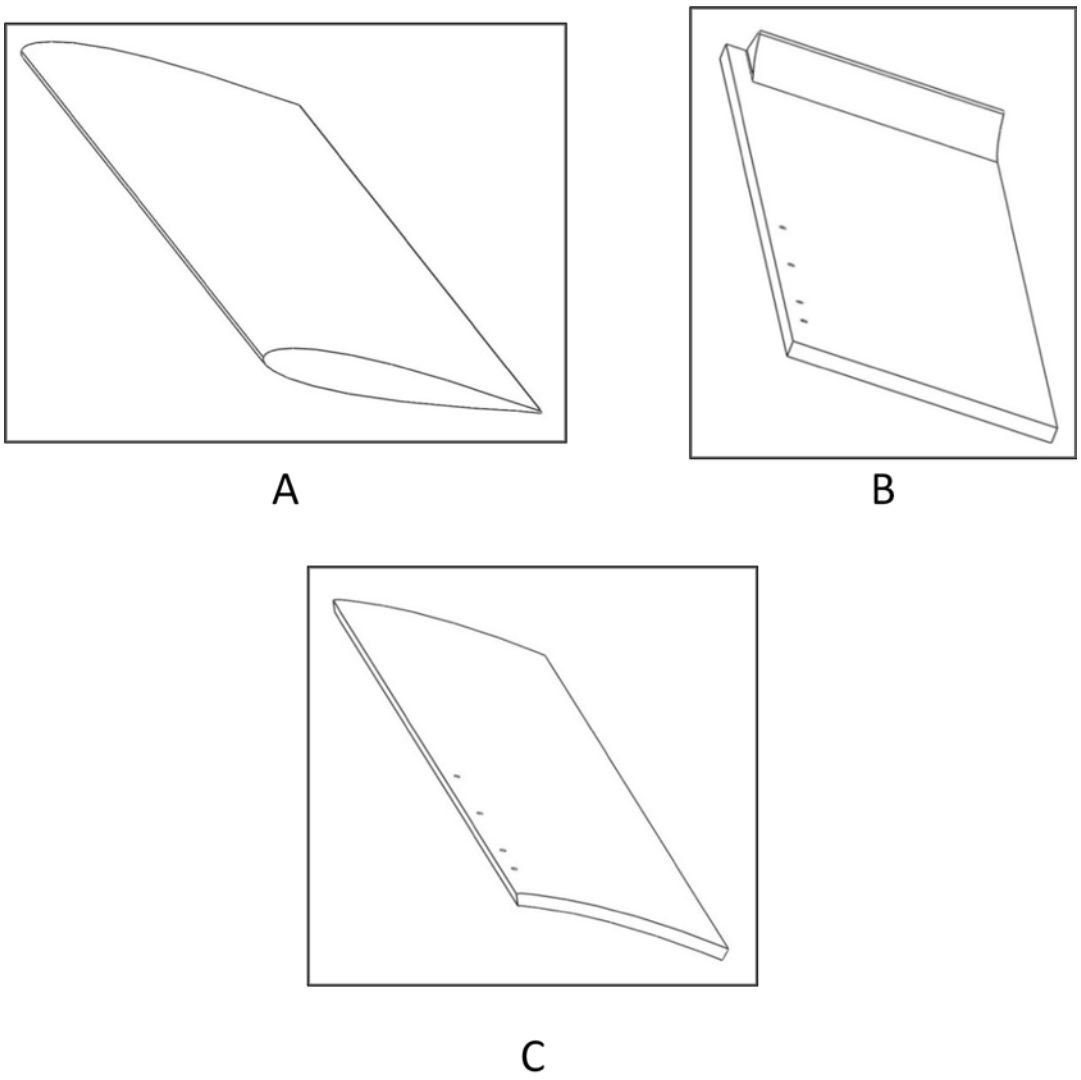

Figure 11: (A) *SolidWorks* model of the NACA 0015 airfoil tested in *FLUENT*
(B) *SolidWorks* model of the first modified scoop tested in *FLUENT*
(C) *SolidWorks* model of the cambered plate tested in *FLUENT*

The lift and drag coefficients were obtained at all angles of attack and rotation for each blade geometry and plotted against the angle of rotation about the θ axis.

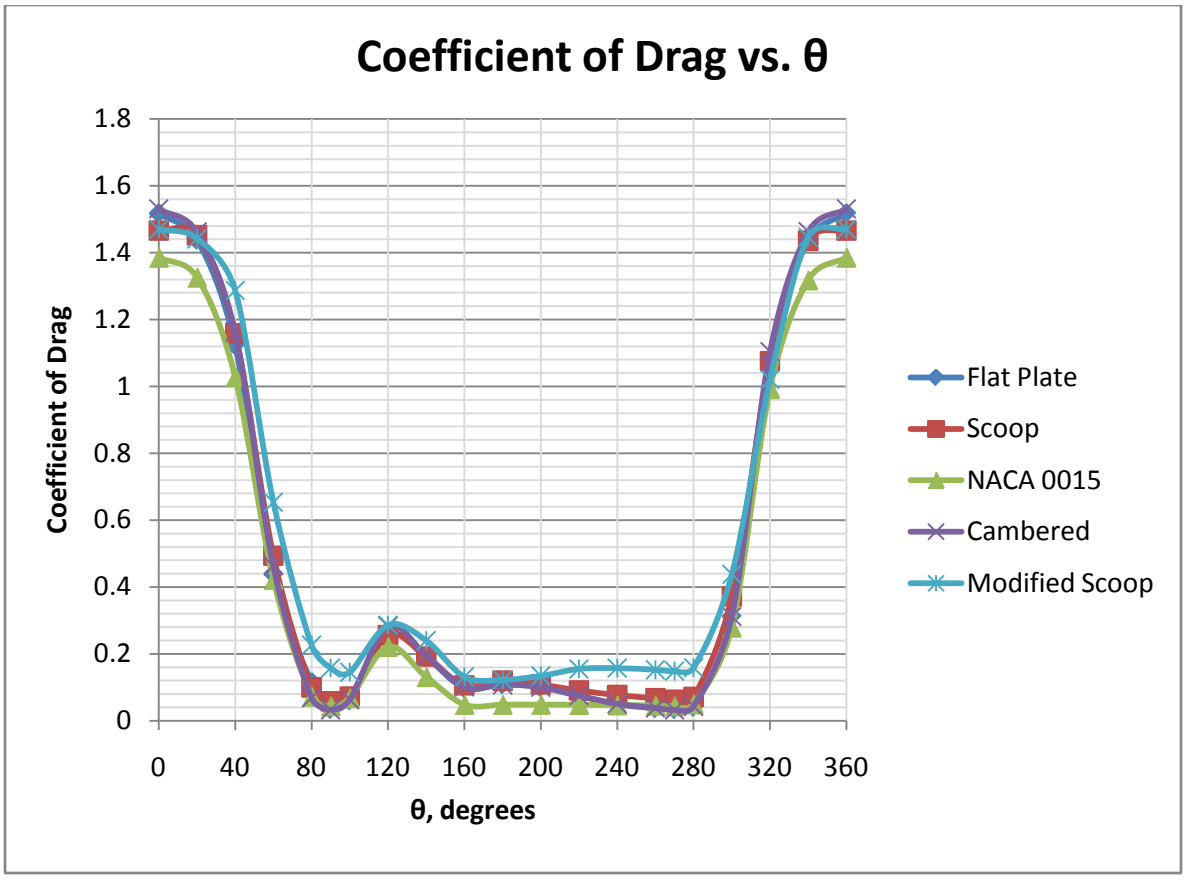

Figure 12: Coefficients of Drag versus Angle of Rotation for Various Blade Profiles

It can be seen that the modified scoop profile had the highest drag in the closed region ($0° \leq \theta \leq 90°$) but also had a high drag in the open region ($180° \leq \theta \leq 270°$). This high drag on the open side would slow down the turbine rotation and consequently affect the overall efficiency. The *NACA 0015* profile had the lowest drag on the open side as expected. While this would be advantageous to the VAWT's efficiency, the team decided that the added benefit was not worth the manufacturing difficulties associated with an airfoil profile. The scoop, cambered, and flat plate designs all had very similar coefficients of drag at similar angles of rotation so it was important to inspect the coefficients of lift for each profile at similar angles of rotation.

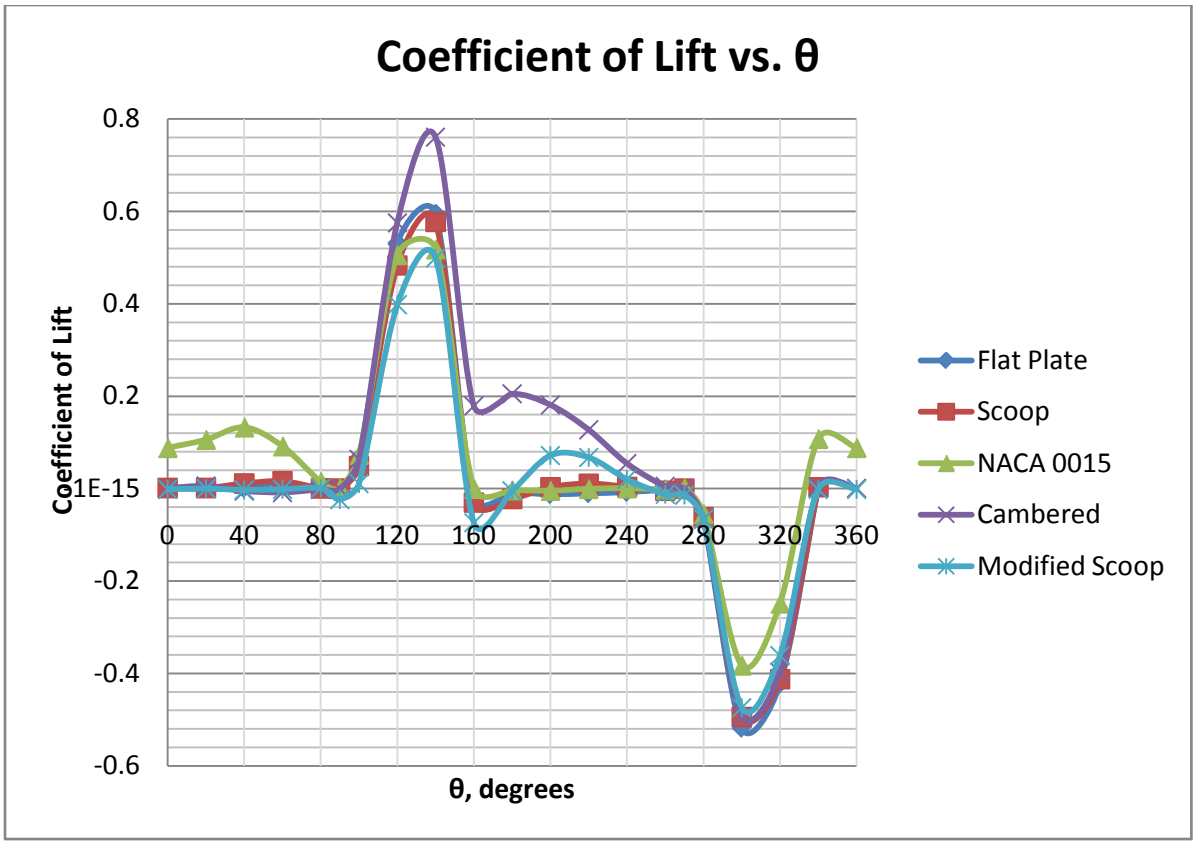

Figure 13: Coefficients of Lift versus Angle of Rotation for Various Blade Profiles

It should be noted that the cambered profile had significantly higher lift than any other blade geometry tested on the open side of the turbine. This was expected to provide extremely advantageous effects on the VAWT's performance because it would keep the blades in the closed and/or opened position(s) longer. The modified scoop also had a high lift on the open side but the group decided with the high drag while on the open side of the turbine that the modified scoop would not suffice as a practical blade geometry to incorporate into the wind turbine design. After studying the data obtained from CFD, the team decided to use the cambered plate blade profile (Detailed information can be found in Appendix B). This geometry had an anticipated ease of fabrication and would provide high drag on the closed side and high lift and low drag on the open side.

Figure 14: *SolidWorks* Model of Cambered Plate Blade Geometry (Camber line of *NACA 4415* Airfoil)

After deciding on the cambered blade, a set of three blades was created and meshed in *GAMBIT* and imported into *FLUENT*. Testing a set of three blades would aid the analysis on the effect of surrounding blades on the

coefficients of lift and drag. CFD was performed on the set of three blades utilizing the method prescribed earlier. The coefficients of lift and drag for the middle of the three blades obtained from this test were plotted against the coefficients of the single blade.

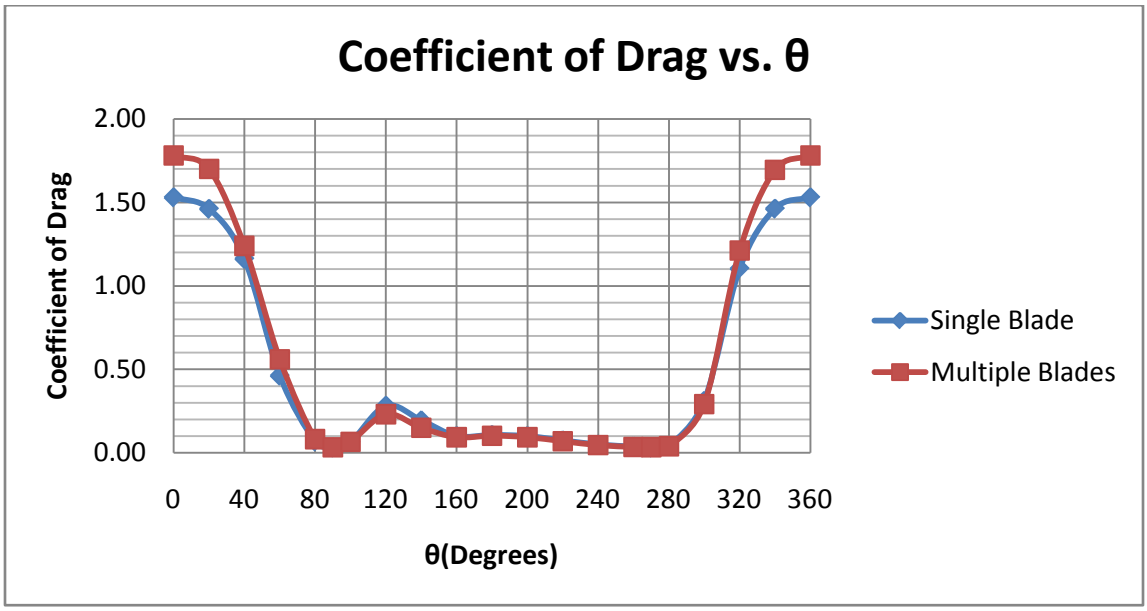

Figure 15: Coefficients of Drag of the Multiple and Single Blades Plotted Against the Angle of Rotation

The middle blade had higher drag on the closed side because the other two blades prevented air from flowing over the top and bottom of the blade. Therefore, the ten interior blades on the closed side of the turbine ($\theta = 0°$) are expected to have drag coefficients of approximately 1.8 while the top and bottom blades are expected to have coefficients of approximately 1.5. This would provide more drag on the closed side than previously expected.

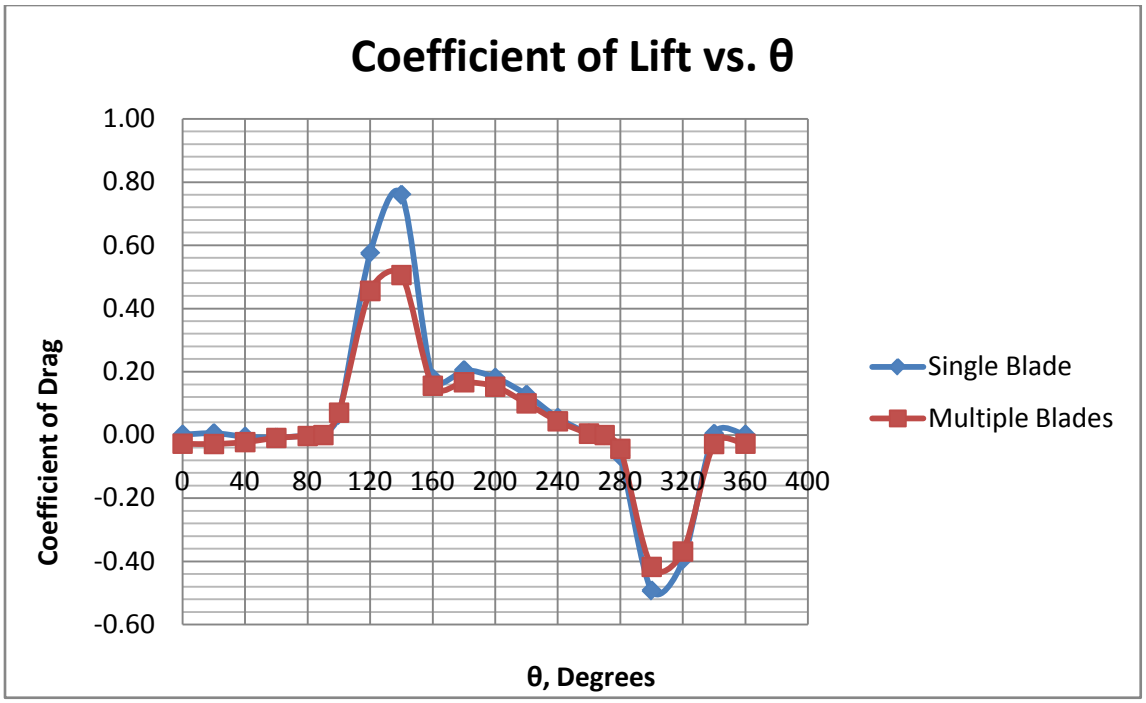

Figure 16: Coefficients of Lift of the Multiple and Single Blades Plotted Against the Angle of Rotation

This figure shows that the middle blade from the set of three has a slightly lower lift on the open side of the turbine, therefore requiring that the ten interior coupled blade pairs rely more heavily on the increased coefficient of drag for the blades on the closed side in order to remain in the steady state position for a longer period of time. That is not to say, however, that the ten interior blades will not experience an increased lift force compared to the 2008 VAWT blades. This differential lift force between interior and exterior blades will not hinder the coupled blade pairs from achieving the steady state position significantly sooner than the flat plate blade geometry.

The use of CFD allowed the VAWT team to gain an understanding of the behavior of the working fluid (i.e., the wind) flow as it interacted with the blades. Without CFD, the team would not have been able to obtain accurate coefficients of lift and drag for each angle of rotation and attack for the numerous blade geometries tested. With all of the data from the *FLUENT* cases, the team confidently chose the cambered plate design as the new VAWT blades.

Material Selection and Fabrication:

Another major consideration for blade design was the selection of an appropriate material. The 2008 design team's blades were fabricated from a ¼ inch flat plate of High Density Polyethylene (HDPE). After some research it was discovered that optimizing the blade material with another plastic proved to be difficult. The plastic selected obtains an extremely high impact strength and fracture toughness. It is also extremely lightweight compared with other plastics, regardless of the moniker "High Density." The most promising potential plastic substitute was Low Density Polyethylene (LDPE); however, the presence of substantial benefits of LDPE over HDPE is minimal. Ultimately, it was decided to incorporate a method of blade construction utilizing fiber-based composite materials. The use of a fiber-based composite allows blades of the desired geometry to

be easily created while fulfilling the requirements of obtaining low weight and relatively high impact strength and fracture toughness. Three major types of fibrous composites were considered: fiberglass, carbon fiber, and Kevlar. Fiber-based composites involve the application of a binder matrix to fiber sheets. As the binder matrix impregnates the fibers and subsequently hardness after several hours, the resulting fiber-based composite material combines the mechanical properties of both the fibers and binder matrix based on the relative amounts of each as a part of the total volume of the object.

Binder Matrix

The design team decided to utilize an epoxy resin as the binder material for the composite blades. Epoxy resins are, "…low-molecular-weight organic liquids containing a number of epoxide groups…" [1]. Epoxy resins are mixed with a hardener, or a curing agent, to polymerize the polymer and form a solid network cross-linked polymer. The chemical reaction between the epoxy resin and the curing agent produces no physical chemical byproduct, but chemical shrinkage does occur accompanied by heat loss from the solution. Three reasons why epoxy resin were selected over other thermosetting polyesters and polymers or thermoplastic resins was because it can cure at room temperature, provides an incredible degree of adhesion to a wide variety of fibers, and it obtains a significant resistance to adverse effects that could be caused by moisture [1]. Secondary reasons why epoxy resin was selected were because it is relatively cheap and it obtains a substantial strength to weight ratio.

Density, g/cm^3	1.2-1.3
Tensile Strength, MPa	55-130
Tensile Modulus, GPa	2.75-4.1
Water Absorption in 24 hr, %	0.08-0.15

Table 2: Typical Properties of Cast Epoxy Resins @ 23°C [1]

US Composites 635 Thin Epoxy Resin with a 4:1 ratio fast epoxy hardener was used to impregnate the reinforcing fibers and bind the composite blades. The 4:1 ratio of epoxy to hardener provides a substantially decreased curing time and also a more rigid and strong laminate once curing completes.

Fibrous Material

Kevlar composites were considered for the blade material because the fibers obtain an extremely high impact resistance, as is evidence from their use in body armor applications. In fact, the impact resistance of Kevlar is the greatest of the three fiber-based materials the team considered as potential candidates for the blade material. It was determined though that, of the three fiber-based materials researched, it is the most troublesome to work and is much more expensive per unit than either carbon fiber or fiberglass, which is why it was removed from final consideration early in the fiber-based composite comparison.

Property, units	Kevlar 29	Kevlar 49	Kevlar 129	Kevlar 149
Density, g/cm^3	1.44	1.44	1.44	1.44
Tensile Strength, MPa	2760	3620	3380	3440
Tensile Modulus, GPa	62	124	96	186
Elongation, %	3.4	2.8	3.3	2.5

Table 3: Typical Mechanical Properties of Kevlar Fibers [1]

Fiberglass was also considered as a potential blade material because of the excellent mechanical properties it obtains, its proven use in many composite structural materials, and its extremely low cost. Although its mechanical properties are not as substantial as Kevlar or carbon fibers, fiberglass was considered due to its potential ability to withstand the fatigue stress caused by the stopping forces the blades experience as they close on one another. The total weight reduction over the 2008 blades would have theoretically been approximately 60%. It should also be noted that the tensile strength data provided in Table 4 represents the virgin values immediately after manufacture and actual strength ratings may vary between 50%-75% of the original virgin values [1].

Property, Units	E-Glass	S-Glass
Density, g/cm^3	2.54	2.49
Tensile Strength, MPa	3448	4585
Tensile Modulus, GPa	72.4	85.5

Table 4: Mechanical Properties of E-Glass and S-Glass Fibers [1]

The design team decided to try and obtain the most substantial strength to weight ratio as possible and therefore also considered carbon fiber as the fibrous material to be utilized for blade fabrication. Carbon-fiber based composite materials exhibit outstanding mechanical properties as well as extreme workability and have a proven track record as paramount materials to utilize in performance criteria when strength to weight ratio is of the utmost importance. Table 5 outlines some of the mechanical properties of the carbon fibers generally utilized in carbon fiber based composite materials [1].

	Precursor Material		
Property, Units	**Polyacrylonitrile (PAN)**	**Pitch**	**Rayon**
Density, g/cm^3	1.77-1.96	2.0-2.2	1.7
Tensile Strength, MPa	1925-6200	2275-4060	2070-2760
Tensile Modulus, GPa	230-595	170-980	415-550
Elongation, %	0.4-1.2	0.25-0.7	---

Table 5: Mechanical Properties of Carbon Fibers [1]

As carbon and E-Glass fiber-based composites were the final two materials considered for blade fabrication, a detailed analysis was completed comparing several properties of each. Table 6 details the relevant information regarding the selection of each fiber reinforced composite as a potential candidate for the turbine blades. The E-glass fiber reinforced blades were a more cost effective choice for blade fabrication; however, the glass fiber reinforced blades would lag behind the performance of the carbon fiber reinforced blades in regards to the composite density, the overall weight of the blades, and the strength of the blades. The carbon fiber blades demonstrate a theoretical tensile strength nearly 1200 psi greater than that exhibited theoretically by the E-glass fiber reinforced blades. The theoretical strength to weight ratio, or specific strength, of the carbon fiber blades also substantially shadows the theoretical strength to weight ratio of the E-glass fiber reinforced composite blades. Ultimately, it was decided to utilize carbon fiber reinforced composite blades over E-glass composite blades. An 11 oz. 2×2 twill weave carbon fiber was selected as the grade of carbon fiber sheet that would be utilized in the fabrication of the blades. The carbon fiber reinforced blades are theorized to be

approximately 35% lighter per blade than the E-glass fiber reinforced blades would have been. A short summary can be found in Table 6 below and the complete analysis can be found in Appendix A.

Table 2: Summary of Blade Materials Selection Analysis							
	Material	Volume Fraction	Total Blade Thickness (in)	Total Composite Blade Density (lbf/in^3)	Weight per blade (lbf)	Tensile Strength (psi)	Cost for Blade Materials
Carbon Fiber Blades	Carbon Fiber Reinforced Composite	13.93%	0.244	0.0084	0.132	26606.951	$535.51
	#1562 Nomex® Honeycomb	86.07%					
E-Glass Fiber Blades	E-Glass Fiber Reinforced Composite	16.47%	0.251	0.0126	0.202	25414.619	$384.21
	#1562 Nomex® Honeycomb	83.53%					

Table 6: Summary of Blade Materials Selection Analysis

Methodology

The final selection of a *NACA 4415* cambered plate blade provided the design team with many options for potential methods of blade construction, but two leading methods presented themselves. One method involved utilizing a female, or negative, mold in which carbon fiber impregnated with the epoxy resin and hardener solution would be inlaid. A Nomex® Honeycomb layer was incorporated and wrapped between the inlaid, impregnated carbon fiber sheet as a means of providing structural integrity and an acceptable working thickness. Information regarding the thicknesses of the blade materials and final blade thickness can be viewed in Appendix A. The sheet was positioned in the mold so that approximately 1 inch of fiber overhang was present on three of the four sides of the blade mold and approximately 5 inches of overhang was present along the remaining 16 inch side. The 5 inch overhang was folded back on top of the Nomex® and an appropriate shape molding weight was applied to the blade while in the mold to assist in maintaining the appropriate geometry. It was noted that the radii the cambered plate blade geometry required for the carbon fiber to adhere was too minute and the carbon fiber insisted on bowing out of the mold. Hence, the shape molding weight was applied. The size of carbon fiber sheets utilized for the female mold method was a 10 inch by 18 inch rectangle. These dimensions were selected so an appropriate amount of fringe would be present after curing completed so the blades would be able to be easily removed from the female mold.

Figure 17: Image Depicting Blade Fabrication Using Female Mold. Carbon Fiber Reinforced Composite w/ Nomex® Honeycomb Core

The other potential method of blade fabrication involved the use of a male, or positive, mold where two layers of epoxy-resin-impregnated carbon fiber sheets were overlaid on the mold. The male mold blade

fabrication technique increased the difficulty of inserting the Nomex® Honeycomb structural support and therefore it was not inserted for fabrication. The team thought that the difficulty would arise in that the Nomex® would not be contained by the walls of a voided volume as was the case with the female mold. Also, the design team postulated that the majority of the mechanical properties of the blades made in the female mold that incorporated the honeycomb insert were derived from the carbon fiber composite, not the Nomex® structural support. This was thought to be a concrete justification for fabrication of a blade on a male mold. However, once a carbon fiber reinforced composite blade was made on the male mold, it was determined that the introduction of the Nomex® honeycomb into the female model significantly increased the strength and toughness of the blades. The team therefore decided to proceed with blade fabrication utilizing the female mold. The images below demonstrate the flexible nature of the two-ply carbon fiber reinforced composite blade made on the male mold and the structure of the two-ply carbon fiber reinforced composite containing a Nomex® honeycomb core made in the female mold.

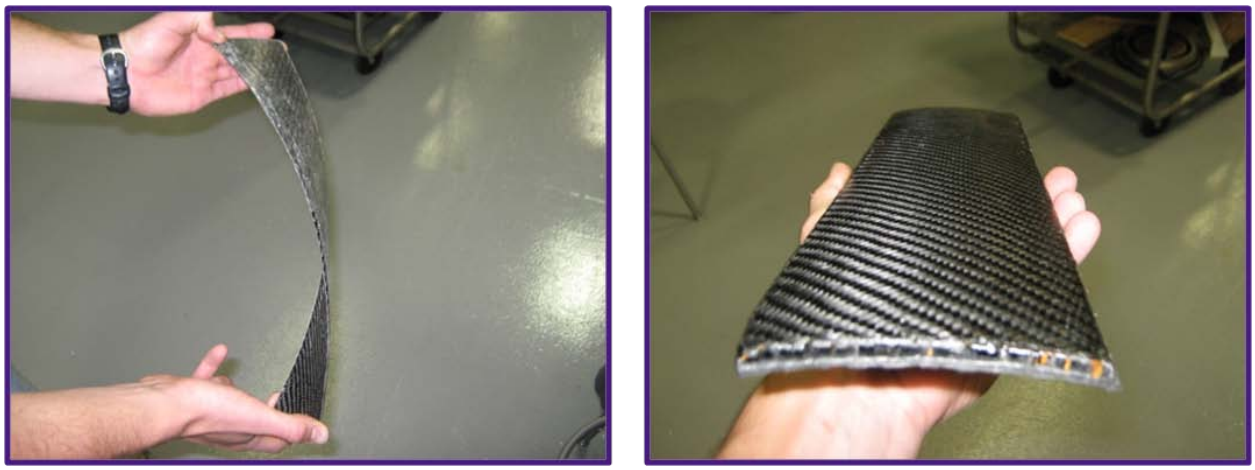

Figure 18: 2-ply CFRC Blade made on Male Mold (Left); 2-ply CFRC Blade w/ Nomex® Honeycomb Core made on Female Mold (Right)

In order to acquire an accurately machined female mold (i.e., the mold obtained the proper blade geometry) the team utilized a Computer Numerical Control (CNC) machine. Some research was conducted to determine what material molds should be machined out of when working with fiber reinforced composites [7]. Main recommendations included medium-density fiberboard (MDF), which is made up of separated fibers, and paraffin wax. More research was conducted on the pricing of the potential mold materials and it was determined that the paraffin wax was more cost effective while MDF was generally more resistant to wear over multiple uses of the mold. A huge benefit that ultimately led the design team to select paraffin wax as the mold material was the convenience of obtaining the material in a short time period. The image on the next page shows in detail one of the paraffin female molds used for blade fabrication with the Nomex® Honeycomb Core inserted.

Figure 19: Paraffin Female Mold Used for Blade Fabrication

The Nomex® honeycomb core inserted into the carbon fiber reinforced composite as a means of amplifying the structural integrity was observed to obtain a preferred bending direction. The material is easily pliable when loaded with moments at the boundaries for a given orientation, which will be termed the transverse direction, and significantly less pliable at a perpendicular orientation, termed the longitudinal direction. After performing a motion study on the flat plate blade geometry utilized on the 2008 VAWT, it was discovered that substantial bending of the blades along the longitudinal direction ($W = 16\ inches$) was occurring during operation of the turbine. As a means of avoiding such phenomena from occurring on the carbon fiber reinforced composite blades, the design team assumed that inserting the Nomex® into the blades such that the preferred bending direction was in the transverse direction would dramatically increase the longitudinal strength. Preventing bending in the longitudinal direction was the major concern, but preventing bending in the transverse direction is also important because any such bending can adversely affect the performance of the blades during operation. To mitigate bending in the both directions, it was hypothesized that if an alternating pattern of Nomex® strips were inserted into the blade such that their preferred bending directions were perpendicular to each other, then the bending of both directions would be minimized. A blade was fabricated in this manner and was observed to obtain minimally improved bending resistance across the transverse direction with no significant changes in the bending resistance across the longitudinal direction. A decision was made to move forward with blade fabrication using a single piece of Nomex® as the core because the opportunity cost of the time required to cut the alternating strips versus the minimally improved mechanical properties was deemed inefficient.

Another major point of concern for composite blade manufacture was brought to the design team's attention during the Final Design Panel Presentation during the Fall 2008 semester. A few design panel members expressed concern over the method by which the blades were to be connected to the connecting rods as well as concerns about blade detachment from the connecting rods during operation. The team thoroughly analyzed the theoretical strength of the carbon fiber reinforced composite blades at the bolt holes where stress concentrations would be present using the Orthotropic Stress Concentration Factor from the Whitney-Nuismer Failure Criteria for Notched Composites [1]. The factor was calculated as $k_T = 2.0217$. In combination with an

expected loading force of approximately 5 lbf, the stress at the bolt holes would be significantly less than the tensile strength of the carbon fiber reinforced composite material. The strength of the four bolts used in attaching the blades were also analyzed and it was determined that the bolts obtain ample strength relative to the shearing area and loading present. Therefore, the team theorized that the blade attachment method is more than adequate for a safe engineering design (Figure 19). This was proven during testing, as not one blade failed mechanically.

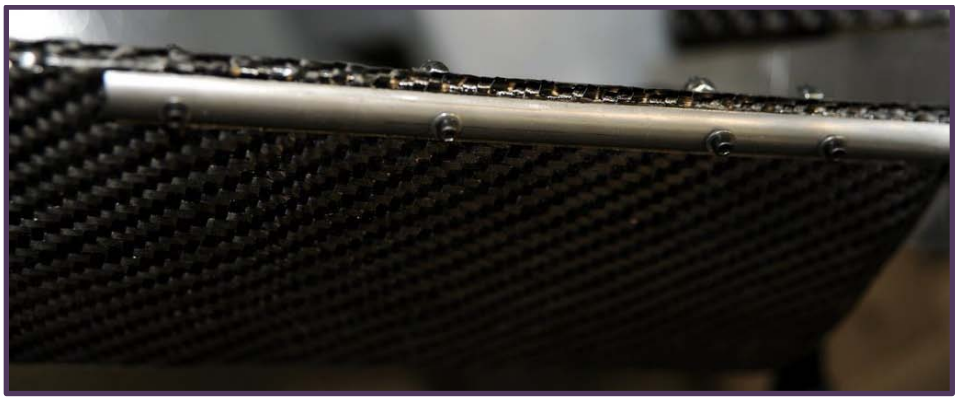

Figure 20: Four Bolt Attachment Method for Blade to Coupling Rods

Table 7 highlights the percent changes of numerous system characteristics of the 2009 vertical axis wind turbine comparative to the 2008 vertical axis wind turbine. Green cells indicated a percent reduction of that system characteristic.

	Individual Blade Weight (lb)	Total (48) Blade Weight (lb)	Rod Weight (lb)	Total (24) Rod Weight (lb)	Θ Inertia (lb*ft^2)	ϕ Inertia (lb*ft^2)	Overall Weight (lb)
2009 VAWT	0.16	7.78	0.21	5.14	5.51	0.01	25.00
2008 VAWT	0.55	26.35	0.41	9.79	17.55	0.04	45.00
Percent Change	**-70%**		**-48%**		**-69%**	**-70%**	**-44%**

Table 7: Table Outlining Percent Changes of Numerous System Characteristics of 2009 vs. 2008 VAWTs [7]

Figure 21 illustrates a completed coupled blade pair assembly modeled in *SolidWorks*. The camber of the blade is also easily visible on both blades, clarifying any misunderstanding of how the lift on the low drag side will positively influence the blade pair to remain in the steady state position longer.

Figure 21: *SolidWorks* Model of Coupled Camber Blade Design

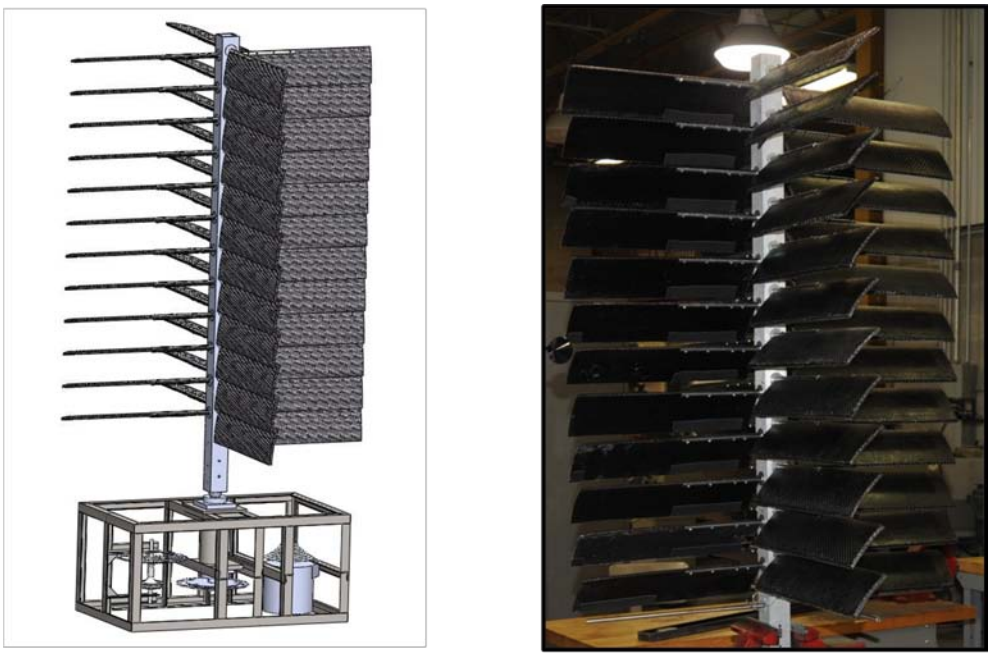

Figure 22: (A) *SolidWorks* Drawing of Complete Turbine Assembly to show Rotor
(B) Actual Completed Turbine Rotor

Results

After initial testing of the 2008 and 2009 rotors began, the design team was able to conduct a preliminary analysis on the acquired data. The most important data relevant to the comparison of the two rotors is the startup speeds of each and the tip speed ratios at different gear ratios for a range of generator circuit resistances.

Obtaining a low startup speed is crucial to the design of a wind turbine because the lower the wind speed required to effectively spin the rotor, the sooner electrical power can begin being generated. As can be

seen in Figure 23, the startup speed of the 2009 VAWT increased as the gear ratio between the shaft and generator increased, which is intuitive because of the greater torque required to rotate a larger gear ratio. It should also be noted that the startup speed also tends to increase at a constant gear ratio whenever the resistance of the electrical circuit containing the generator decreases. For a constant gear ratio the startup speed increases as the electrical resistance decreases because the reverse torque, or back electromagnetic force, applied by the generator increases as a result of decreasing the resistance. The correlation between the backwards electromagnetic force and resistance is direct and easily explained. Decreasing the electrical resistance in the generator circuit allows for more current to flow through the circuit. Increases in current flow through a generator circuit significantly increases the torque required to spin the generator. If the electrical resistance is increased, however, the current is limited and the backwards electromagnetic force decreases, thus decreasing the input torque required to rotate the generator and consequently lowering the startup speed of the wind turbine.

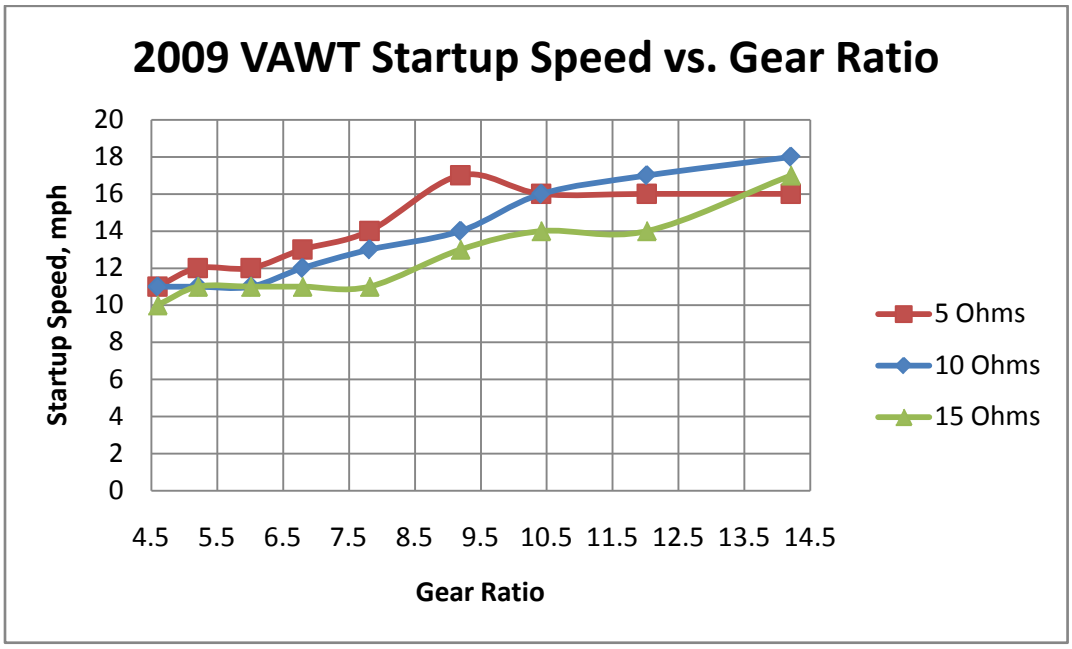

Figure 23: 2009 VAWT Startup Speeds (mph) at Different Gear Ratios for Various Circuit Resistances (Ω)

The tip speed ratio provides insight into approximately how much energy the rotor extracts from the incident wind. RPM data was recorded for both rotors at numerous wind speeds, ranging from startup speed to as near the maximum operating constraint of 50 miles per hour the team could maintain. The two plots below show the relationships between rotor RPM and blade TSR versus wind speed for a freewheeling configuration. A freewheeling configuration means that the transmission was disconnected from the rotor and therefore it was not driving the generator. This test was done to obtain information regarding the ideal rotor RPM and TSR for both the 2008 and 2009 rotors and determine which rotor's performance was paramount. It is obvious from the data that the 2009 VAWT rotor was more aerodynamically efficient under all wind speeds when no load is attached to the rotor.

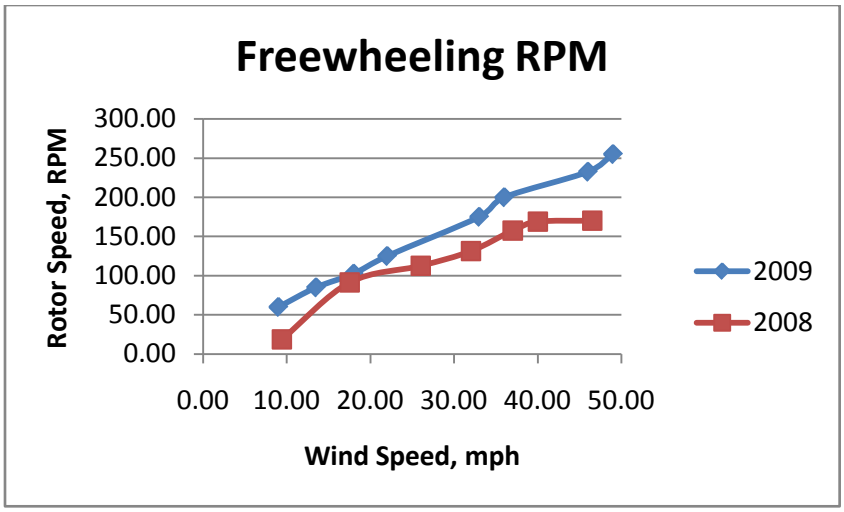

Figure 24: Freewheeling RPM (i.e., disconnected from transmission) of Rotors at Various Wind Speeds

Some interesting information was discovered when the TSR was backed out from the RPM information utilizing the following formula:

$$TSR = \frac{RPM * \left(\frac{2\pi}{60}\right) * r_{tip}}{V_W}$$

where:

$$r_{tip} = Radius\ of\ blade\ tip\ from\ vertical\ axis\ (m) \quad V_W = Incident\ wind\ speed\ velocity\ (m/s)$$

It should be noted that the TSR of both rotors drops at increased incident wind speeds. One possible explanation for this behavior could be attributed to the extreme turbulence thought to be present and adversely affecting the blades at the rear of the turbine for $70° \leq \theta \leq 110°$.

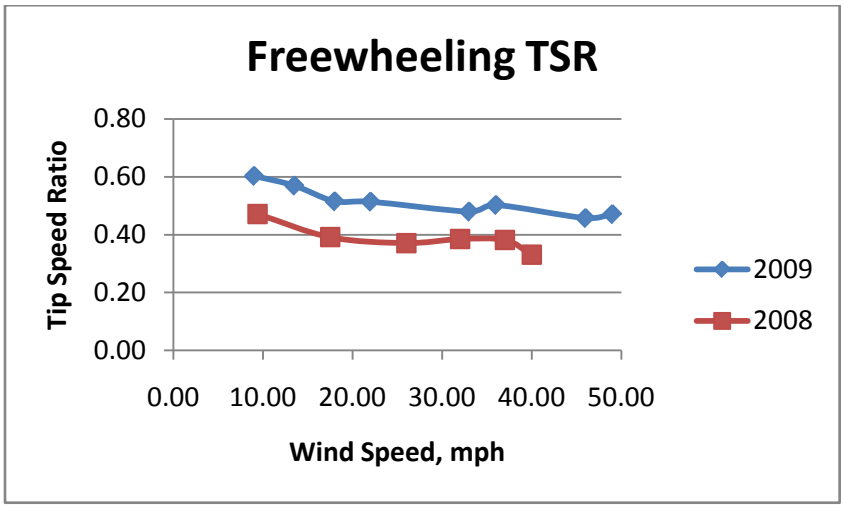

Figure 25: Freewheeling TSR (i.e., disconnected from transmission) of Rotors at Various Wind Speeds

The subsequent two plots illustrate the behavior of the 2008 and 2009 rotor RPM and TSR versus wind speed when a known, constant load is applied to the rotor through its connection to the transmission and the presence of a generator load. The following data represents measurements taken for tests in which the transmission was in first gear and 10 ohm resistance was applied to the generator circuit. It can be seen that the two rotors behave rather similarly at low wind speeds, yet as the incident wind speed reaches the mid range of operating speeds the 2008 rotor obtains higher RPM readings. At first this perplexed the team, but they determined that the greater mass moment of rotational inertia of the 2008 rotor over that of the 2009 rotor was the reason the 2008 rotor was obtaining higher sustained RPM values. Once the 2008 rotor attained significant angular momentum, the momentum only benefitted the rotor as it is more difficult to slow an object with more inertia. At the top end of the testing range, the two rotors did merge so it was hypothesized that if the wind speed were to be increased and tested above 50 miles per hour, then the two rotors would behave relatively similarly.

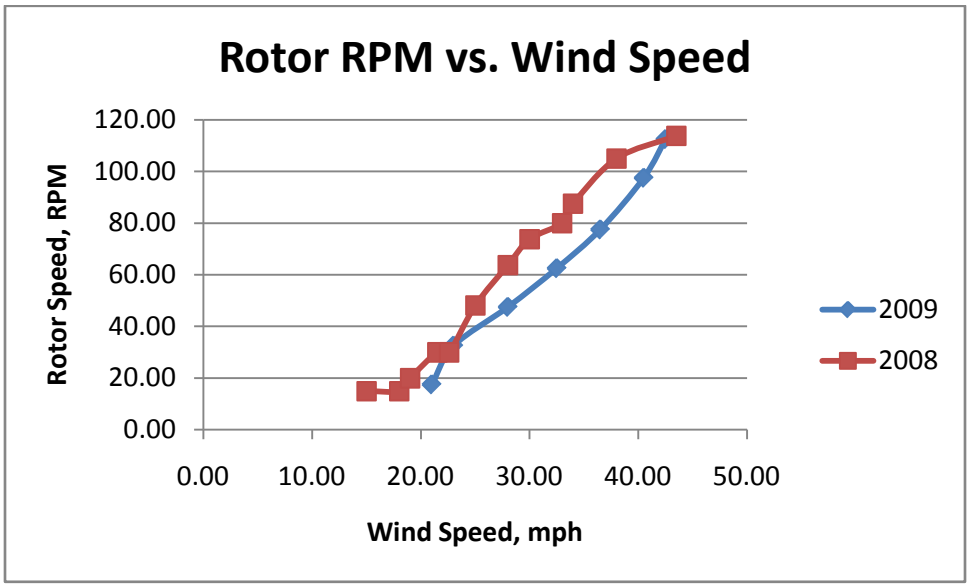

Figure 26: RPM of Rotors at Various Wind Speeds. Turbine configured in Gear 1 (Gear ratio = 4.6) at 10 Ω circuit resistance.

Valuable information regarding the TSR can also be obtained from Figure 28, which shows the TSR of the two rotors from the tests conducted in Figure 27. Remember from Figure 26 that the TSR of the freewheeling 2009 rotor decreased from a maximum of approximately 0.58 at low wind speeds rather constantly to 0.47. The 2008 rotor also followed this trend but with lesser TSR values. However, the 2008 rotor obtained greater TSR values for the test where the transmission was connected and a generator load was applied. This was not a surprise because the 2008 rotor RPM values were greater, but the fact that the TSR increased as wind speed increased was a surprise. With the presence of a gear and applied generator load, the rotors have to overcome internal forces of friction and increased torque required to spin the gear ratio. The fact that the rotors start at similar TSRs is intuitive, as is the greater TSR for the 2008 rotor over the 2009 rotor. At higher RPM, the 2008 has increased angular momentum and is less affected by the internal forces acting on the shaft and is thus able to maintain consistently higher RPM and consequently consistently higher TSR values.

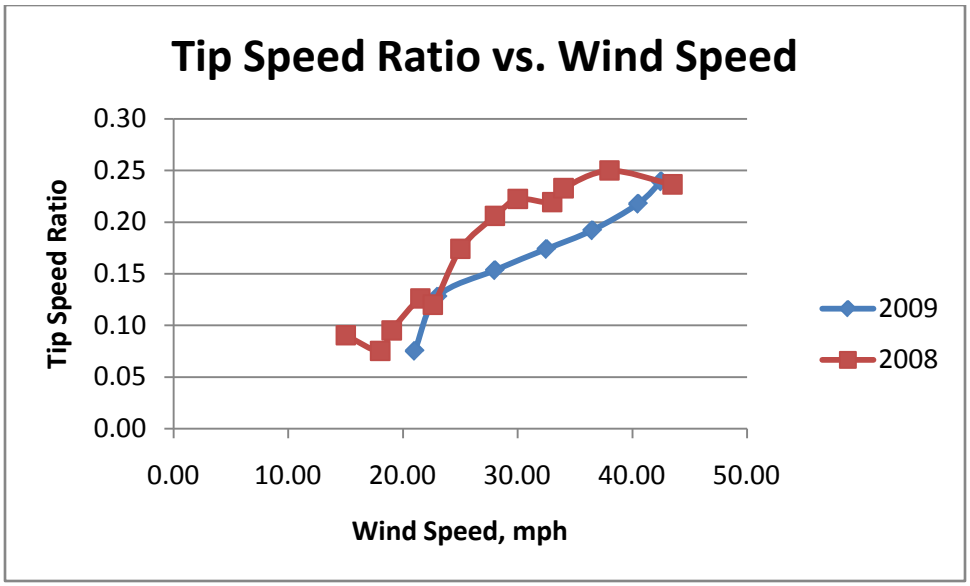

Figure 27: TSR of Rotors at Various Wind Speeds. Turbine configured in Gear 1 (Gear ratio = 4.6) at 10 Ω circuit resistance.

Conclusion

Dr. James R. Bailey's concept for a vertical axis wind turbine provides a system that transforms energy from a natural resource that is clean and plentiful. Past rises in fossil fuel prices and the concept of "green" engineering solutions have provided the impetus for increased research of alternative energy solutions, such as wind energy. The dominant reason that drag-based vertical axis wind turbines, like the Savonius and the Darrieus, are not produced commercially is because of the low overall efficiencies that these turbines demonstrate compared to lift-based horizontal axis wind turbines. The main goal of this year's vertical axis wind turbine team was to increase the overall efficiency from last year's 13% to a range of 15-20%. The 2009 design team has conducted a preliminary data analysis of efficiency readings from testing. The design team has been unable to replicate the results reported by the 2007-2008 design team. Several factors could be the cause of efficiency reading incompatibilities between the two data sets including changes in the transmission design, calculation errors, or testing inconsistencies. A final efficiency analysis will be conducted once testing is completed in order to determine whether or not the 2009 VAWT team will be able to obtain the efficiency readings reported by the 2008 VAWT team and if the 2009 VAWT has overall greater efficiency.

It was thought that by performing computational fluid dynamics on different blade geometries, in conjunction with applying Newtonian mechanics for a dynamic analysis of the blades, the optimum blade geometry would be found. This very well may be the case, as a motion study of the cambered plate blades compared to the 2008 team's flat plate blade geometry shows that the blades are staying closed longer on the high drag side of the turbine and remaining open longer on the low drag side of the turbine. Also, the 2009 rotor (i.e., full assembly of main shaft, connecting rods, and blades) obtained significantly higher RPM values versus the 2008 rotor at a wide range of wind speeds when allowed to rotate with no load applied. However, when the same constant load was applied to the two turbines, the 2008 rotor obtained higher RPM values at the top end of the operating wind speed range. The team has postulated that though the 2009 blades are performing more efficiently in terms of lift and drag coefficients, the greater rotational inertia of the 2008 turbine could be

benefiting it once the turbine achieves high RPM. It can be hypothesized that a combination of a turbine obtaining a high rotational inertia and cambered plate blades (aerodynamic blades) could potentially lead to a more overall efficient turbine.

References

1) Agarwal, Bhagwan D., Lawrence J. Broutman, K. Chandrashekhara. *Analysis and Performance of Fiber Composites*. 3rd ed. Hoboken: John Wiley & Sons, Inc.
2) Airfoil: NACA 0015. 1981. Sandia National Laboratories. 10/29/08. http://www.cyberiad.net/library/airfoils/foildata/n0015cd.htm.
3) Airfoil: NACA 0015. 1981. Sandia National Laboratories. 10/29/08. http://www.cyberiad.net/library/airfoils/foildata/n0015cl.htm.
4) Budynas, Richard G. and J. Keith Nisbett. *Shigley's Mechanical Engineering Design*. 8th ed. New York: McGraw Hill, 2008.
5) Low Wind Permanent Magnet Alternator. 2007. WindBlue Power LLC. 11/7/08 http://www.windbluepower.com/.
6) Louisiana State University Mechanical Engineering Department Senior Design 2007-2008 Final Report: Vertical Axis Wind Turbine.
7) Louisiana State University Mechanical Engineering Department Senior Design 2008-2009 Semester Report: Vertical Axis Wind Turbine.
8) McMaster-Carr. 11/7/08 www.McMaster.com
9) Vertical Windmill Blades. 2009. The Creative Science Center. 4/21/09. http://www.creative-science.org.uk/projects/wind/ver_windmill_blades.gif.

Appendix A

Area of blade materials needed:	
3072	in^2
1.982	m^2

Vendor	Material	Thickness (mils)	Thickness (m)	Density (kg/m^3)	Unit Cost	Total Cost
Fiberglast	#1562 Nomex® Honeycomb Sandwich Cores (40" x 100")	0.21	0.0053	28.833	$174.95 /sheet	$174.95
US Composites	11oz '1st Quality' 2x2 T will Weave Carbon Fiber (50" width)	0.017	0.0004	1760	$43.50 /yard	$217.50
US Composites	EPOX-635413 (1 gallon resin, 1 quart hardener)			1102.403	$60.00 /Package	$60.00
	EPX-P41 (4-1 ratio pumps)				$6.25 /Set of 2	$6.25
US Composites	FR-1157A (1" diameter, 7" length)				$11.80 /Roller	$11.80

$470.50	**Subtotal**
$32.06	**Tax**
$32.95	**Shipping**
$535.51	**Total**

Vendor	Material	Thickness (mils)	Thickness (m)	Density (kg/m^3)	Unit Cost	Total Cost
Fiberglast	#1562 Nomex® Honeycomb Sandwich Cores (40" x 100")	0.21	0.0053	28.833	$174.95 /sheet	$174.95
US Composites	18oz E-glass Plain Weave (38" wide)	0.0207	0.0005	2540	$9.35 /yard	$56.10
US Composites	EPOX-6354(1&3) (1.25 gallon resin, 1.25 quart hardener)			1102.403	$80.00 /Package	$80.00
	EPX-P41 (4-1 ratio pumps)				$6.25 /Set of 2	$6.25
US Composites	FR-1157A (1" diameter, 7" length)				$11.80 /Roller	$11.80

$329.10	**Subtotal**
$22.16	**Tax**
$32.95	**Shipping**
$384.21	**Total**

Appendix B (NACA 4415 Camber Profile)

NACA 4415										
Surface Point Number	Upper Surface				Lower Surface				Camber Line	
	x (% of CL)	y (% of CL)	x(CL=4)	y(CL=4)	x (% of CL)	y(% of CL)	x(CL=4)	y(CL=4)	x(CL=4)	y(CL=4)
1	0.0125	0.0307	0.05	0.1228	0.0125	-0.0179	0.05	-0.0716	0.05	0.0256
2	0.025	0.0417	0.1	0.1668	0.025	-0.0248	0.1	-0.0992	0.1	0.0338
3	0.05	0.0574	0.2	0.2296	0.05	-0.0327	0.2	-0.1308	0.2	0.0494
4	0.075	0.0691	0.3	0.2764	0.075	-0.0371	0.3	-0.1484	0.3	0.064
5	0.1	0.0784	0.4	0.3136	0.1	-0.0398	0.4	-0.1592	0.4	0.0772
6	0.15	0.0927	0.6	0.3708	0.15	-0.0418	0.6	-0.1672	0.6	0.1018
7	0.2	0.1025	0.8	0.41	0.2	-0.0415	0.8	-0.166	0.8	0.122
8	0.25	0.1092	1	0.4368	0.25	-0.0398	1	-0.1592	1	0.1388
9	0.3	0.1125	1.2	0.45	0.3	-0.0375	1.2	-0.15	1.2	0.15
10	0.4	0.1125	1.6	0.45	0.4	-0.0325	1.6	-0.13	1.6	0.16
11	0.5	0.1053	2	0.4212	0.5	-0.0272	2	-0.1088	2	0.1562
12	0.6	0.093	2.4	0.372	0.6	-0.0214	2.4	-0.0856	2.4	0.1432
13	0.7	0.0763	2.8	0.3052	0.7	-0.0155	2.8	-0.062	2.8	0.1216
14	0.8	0.0555	3.2	0.222	0.8	-0.0103	3.2	-0.0412	3.2	0.0904
15	0.9	0.0308	3.6	0.1232	0.9	-0.0057	3.6	-0.0228	3.6	0.0502
16	0.95	0.0167	3.8	0.0668	0.95	-0.0036	3.8	-0.0144	3.8	0.0262
17	1	0.0016	4	0.0064	1	-0.0016	4	-0.0064	4	0
18	1	0	4	0	1	0	4	0	4	0

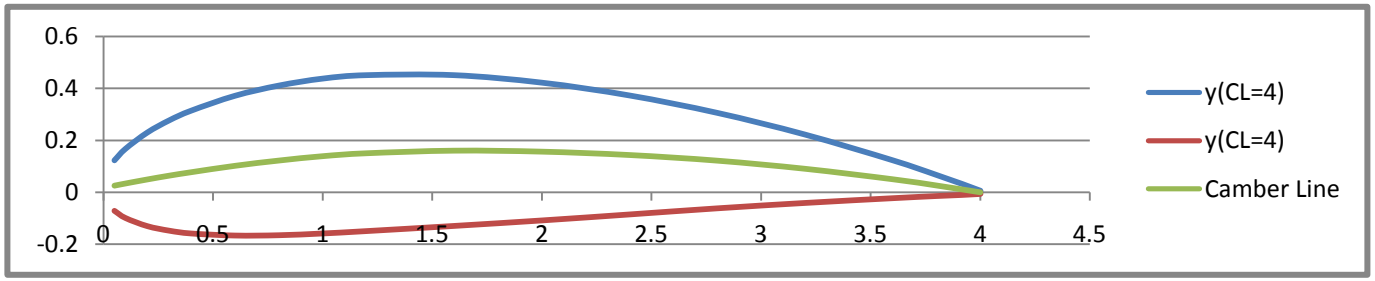

Appendix C

```
%This MATLAB code determines the position of a specified point on one of the
%blades in a coupled pair, thus the position of both blades during a complete
%revolution about the theta axis.
R=1;
W=16;
CL=4;

L=0;
y=W;
z=CL;
for(y=0:16:16)
    for(z=0:4:4)
        for(theta=0:.01:2*pi)
            if (theta<=2*pi)
                phi=2*pi-theta;
            end
            if (theta<=3*pi/2)
                phi=pi/2;
            end
            if (theta<=pi)
                phi=theta-pi/2;
            end
            if (theta<=pi/2)
                phi=0;
            end
            rx=-(R*sin(theta)+y*sin(theta)-z*sin(phi)*cos(theta));
            ry=R*cos(theta)+y*cos(theta)+z*sin(phi)*sin(theta);
            rz=L-z*cos(phi);
            plot3(rx,ry,rz);
            hold on;
        end
    end
end
```

Appendix D

```
%This MATLAB code determines the value of phi as a function of the incident
%wind speed and the angular displacement, theta, about its axis.
function [phi,dphi]=getphi(theta)
global Vw_mph
global dtheta

V=Vw_mph(1,1);
theta_closed=(1.688*V-33.252)*pi/180;
theta_open=(-.1666*V+64.473)*pi/180;

if nargin==0
    fprintf('Must input theta!\n')
else
    while theta>2*pi
        theta=theta-2*pi;
    end
    if theta<=(pi/2+theta_closed);
        phi=0;
        dphi=0;
    else if theta<=(pi/2+theta_open);
            phi=-pi/2*theta/(theta_open-theta_closed)+pi/2*(pi/2+...
                theta_closed)/(theta_open-theta_closed);
            dphi=(pi/2)/((theta_closed-theta_open)/dtheta);
        else if theta<=(3*pi/2+theta_closed);
                phi=-pi/2;
                dphi=0;
            else if theta<=(3*pi/2+theta_open);
                    phi=pi/2*theta/(theta_open-theta_closed)-...
                        pi/2*(3*pi/2+theta_open)/(theta_open-theta_closed);
                    dphi=(pi/2)/((theta_open-theta_closed)/dtheta);
                else
                    phi=0;
                    dphi=0;
                end
            end
        end
    end
end
```

Appendix E

```
%This MATLAB code determines the relative velocity of the center of mass of
%a blade during an entire revolution of the turbine shaft, taking into
%consideration the angles theta and phi. The equation is the first time
%derivative of Equation 2 that was derived in the dynamic analysis.
function Vrel=getVrel(theta,phi,dphi)
global R
global t
global W
global CL
global dtheta
global Vw

%Coordinates of CG of blade couple being analyzed
x=0*t;
y=.5*W;
z=.5*CL;

if nargin==0
    fprintf('Must input theta,phi,and dphi!\n');
else
    while theta>2*pi
        theta=theta-2*pi;
    end
    %Vrel of CG of blade
    Vbx=-x*sin(phi)*cos(theta)*dphi-x*cos(phi)*sin(theta)*dtheta...
        -z*cos(phi)*cos(theta)*dphi+z*sin(phi)*sin(theta)*dtheta...
        -y*cos(theta)*dtheta-R*cos(theta)*dtheta;
    Vby=-x*sin(phi)*sin(theta)*dphi+x*cos(phi)*cos(theta)*dtheta...
        -y*sin(theta)*dtheta-z*cos(phi)*sin(theta)*dphi...
        -z*sin(phi)*cos(theta)*dtheta-R*sin(theta)*dtheta;
    %Vbz=-x*cos(phi)*dphi+z*sin(phi)*dphi;

    Vw_bx=-Vw(1,1)-Vbx;
    Vrel=sqrt(Vw_bx^2+Vby^2);
end
```

Appendix F

```
%This MATLAB code determines the projected area of the blade as seen from
%the perspective of the incident wind. This is integral in the
%calculation of the lift and drag forces acting on a given blade profile.
function Aproj=getAproj(theta,phi)
global W
global CL
global t

if nargin==0
    fprintf('Need to input theta and phi!\n');
else
    while theta>2*pi
        theta=theta-2*pi;
    end
    %Quadrant 1 and 4
    if (theta<=pi/2||theta>3*pi/2)
        Aproj=W*CL*cos(phi)*cos(theta)+t*W*-sin(phi)*cos(theta);

        %Quadrant 2 and 3
    else if (theta<=3*pi/2)
            Aproj=W*CL*cos(phi)*-cos(theta)+t*W*-sin(phi)*-cos(theta);
        end
    end
end
```

Appendix G

```
%This MATLAB code determines the lift and drag coefficients for a flat
%plate blade geometry at characteristic combinations of theta and phi for a
%complete revolution of the turbine shaft.
function [Cd,Cl]=getCdCl_AR4(theta,phi)

if nargin==0
    fprintf('Need to input theta, & phi!\n');
else
    while theta>2*pi
        theta=theta-2*pi;
    end
    phinew=phi+pi/2;
    if theta<=40*pi/180
        Cd=-1.2492*(phinew^2)+0.1544*phinew+1.6871;
    else if theta<=80*pi/180
            Cd=0.3281*(phinew^2)-2.2683*phinew+2.6096;
        else if theta<=100*pi/180
                Cd=1.3076*(phinew^2)-4.1542*phinew+3.3334;
            else if theta<=140*pi/180
                    Cd=-1.0869*(phinew^2)+4.6864*phinew-4.8024;
                else if theta<=180*pi/180
                        Cd=0.3081*(phinew^2)-1.8035*phinew+2.7266;
                    else if theta<=270*pi/180
                            Cd=-0.0182*(phinew^5)+0.3384*(phinew^4)-...
                                2.4437*(phinew^3)+8.5491*(phinew^2)-...
                                14.433*phinew+9.4614;
                        else if theta<=300*pi/180
                                Cd=1.3608*(phinew^2)-13.027*phinew+31.205;
                            else
                                Cd=0.041*(phinew^3)-2.1942*(phinew^2)+...
                                    22.509*phinew-63.283;
                            end
                        end
                    end
                end
            end
        end
    end
    if theta<=80*pi/180
        Cl=0.9882*(phinew^2)-2.8679*phinew+2.0667;
    else if theta<=100*pi/180
            Cl=0.1273*(phinew^4)-0.3062*(phinew^3)+0.2509*(phinew^2)-...
                0.0649*phinew-0.0601;
        else if theta<=160*pi/180
                Cl=-0.4704*(phinew^3)+1.5064*(phinew^2)+0.6395*phinew-...
                    3.1326;
            else if theta<=280*pi/180
                    Cl=-0.143*(phinew^6)+3.2122*(phinew^5)-...
                        29.846*(phinew^4)+146.87*(phinew^3)-...
                        403.93*(phinew^2)+589.08*phinew-355.9;
                else if theta<=320*pi/180
                        Cl=2.0023*(phinew^2)-21.412*phinew+56.771;
                            else
                                Cl=-1.2418*(phinew^2)+15.166*phinew-46.327;
                    end
                end
            end
        end
    end
end
end
```

Appendix H

```
%This MATLAB code determines the Reynold's number of the flow over the
%blades for a given incident wind speed. The Reynold's number is considered
%constant and is calculated with the chord length as the characteristic
%length. This is important data necessary for conglomeration with FLUENT
%runs. This helps determine what sort of regime, laminar or turbulent, the
%fluid is flowing in and therefore what type of solver should be utilized
%in FLUENT.
function Re=getReynolds(Vrel)
global CL
global rhoa
global mua

if nargin==0
    fprintf('Need to input relative velocity!\n');
else
    Re=(rhoa*Vrel*CL)/mua;
end
```

Appendix I

```
%This MATLAB code was utilized to print out the relative velocity for
%characteristic combinations of theta and phi for a revolution around the
%turbine shaft. The data was utilized for blade construction in GAMBIT and
%inputs into FLUENT. Though coded for 1 degree intervals, the tests in
%FLUENT were conducted at 20 degree intervals as a means of limiting the
%time spent computing complex fluid flow simulations.
clc;
clear all;

global Vw_mph
global R
global W
global CL
global t
global L
global dtheta
global Vw
global rhoa
global mua

%Gravitational acceleration in m/s^2
g=9.8066;

%Dimensions measured in meters
R=1/12*0.3048;
W=16/12*0.3048;
CL=4/12*0.3048;
t=0.25/12*0.3048;
L=0*0.3048;
H=45/12*0.3048;

%Aspect ratio
AR=W/CL;

%Density measured in kg/m^3
rhoa=1.225;
rhob=945;

%Dynamic Viscosity in (N*s)/m^2
mua=1.98e-05;

%Wind speed input in mph and converted to m/s
wind=-30;

Vw_mph=[wind 0];
if Vw_mph(1,1)<0
    Vw_mph(1,1)=-Vw_mph(1,1);
end
Vw=Vw_mph*1.46666667*.3048;
```

```
%The Tip Speed Ratio
TSR=((W*12/.3048)*(2*pi/60)*(3.923625*Vw_mph(1,1)...
    -0.43125))/(Vw_mph(1,1)*17.6)
Vtip=TSR*Vw(1,1);

%Shaft angular velocity equal to Vtip/Rtip
dtheta=Vtip/(R+W);

for i=1:91;
    theta(i)=(i-1)*pi/180;
    theta2(i)=theta(i)+pi/2;
    theta3(i)=theta(i)+pi;
    theta4(i)=theta(i)+3*pi/2;

    %Call needed variables from their programs
    [phi(i) dphi(i)]=getphi(theta(i));
    Vrel(i)=getVrel(theta(i),phi(i),dphi(i));
    Re(i)=getReynolds(Vrel(i));
    fprintf('theta=%11.5f   phi=%10.5f
Vrel=%10.5f\n',theta(i)*180/pi,(phi(i)+pi/2)*180/pi,Vrel(i));

    [phi2(i) dphi2(i)]=getphi(theta2(i));
    Vrel2(i)=getVrel(theta2(i),phi2(i),dphi2(i));
    Re2(i)=getReynolds(Vrel2(i));
    fprintf('theta2=%10.5f   phi2=%9.5f
Vrel2=%9.5f\n',theta2(i)*180/pi,(phi2(i)+pi/2)*180/pi,Vrel2(i));

    [phi3(i) dphi3(i)]=getphi(theta3(i));
    Vrel3(i)=getVrel(theta3(i),phi3(i),dphi3(i));
    Re3(i)=getReynolds(Vrel3(i));
    fprintf('theta3=%10.5f   phi3=%9.5f
Vrel3=%9.5f\n',theta3(i)*180/pi,(phi3(i)+pi/2)*180/pi,Vrel3(i));

    [phi4(i) dphi4(i)]=getphi(theta4(i));
    Vrel4(i)=getVrel(theta4(i),phi4(i),dphi4(i));
    Re4(i)=getReynolds(Vrel4(i));
    fprintf('theta4=%10.5f   phi4=%9.5f
Vrel4=%9.5f\n',theta4(i)*180/pi,(phi4(i)+pi/2)*180/pi,Vrel4(i));
    fprintf('\n');
end
```